Front. Phys., 2014, 9(2): 170–193
DOI 10.1007/s11467-013-0360-6

REVIEW ARTICLE

Single photon sources with single semiconductor quantum dots

Guang-Cun Shan[1,2,*], **Zhang-Qi Yin**[3], **Chan Hung Shek**[1], **Wei Huang**[4,†]

[1] *Department of Physics and Materials Science, City University of Hong Kong, Hong Kong SAR, China*
[2] *The Fu Foundation School of Engineering and Applied Science, Columbia University, New York, NY 10027, USA*
[3] *The Institute for Interdisciplinary Information Sciences (IIIS), Tsinghua University, Beijing 100084, China*
[4] *Singapore-Jiangsu Joint Research Center for Organic/Bio-electronics and Information Displays and Institute of Advanced Materials, Nanjing University of Technology, Nanjing 211816, China*

Corresponding authors. E-mail: *gshan2-c@my.cityu.edu.hk, †wei-huang@njut.edu.cn

Received February 24, 2013; accepted May 30, 2013

In this contribution, we briefly recall the basic concepts of quantum optics and properties of semiconductor quantum dot (QD) which are necessary to the understanding of the physics of single-photon generation with single QDs. Firstly, we address the theory of quantum emitter-cavity system, the fluorescence and optical properties of semiconductor QDs, and the photon statistics as well as optical properties of the QDs. We then review the localization of single semiconductor QDs in quantum confined optical microcavity systems to achieve their overall optical properties and performances in terms of strong coupling regime, efficiency, directionality, and polarization control. Furthermore, we will discuss the recent progress on the fabrication of single photon sources, and various approaches for embedding single QDs into microcavities or photonic crystal nanocavities and show how to extend the wavelength range. We focus in particular on new generations of electrically driven QD single photon source leading to high repetition rates, strong coupling regime, and high collection efficiencies at elevated temperature operation. Besides, new developments of room temperature single photon emission in the strong coupling regime are reviewed. The generation of indistinguishable photons and remaining challenges for practical single-photon sources are also discussed.

Keywords single-photon source, quantum dot (QD), quantum optics, photon correlation

PACS numbers 42.50.Dv, 42.50.Ct, 42.50.Gy, 42.50.Pq, 78.67.-n, 78.67.Hc

Contents

1 Introduction

Developing single photon sources has gained considerable interest both for fundamental aspects, such as light-

© Higher Education Press and Springer-Verlag Berlin Heidelberg 2014

matter interaction [1–5] and for important applications in quantum information science [2, 4, 6]. In particular, single photon sources could lead to practical ways of realizing scalable photonic quantum computing [6], unconditional quantum cryptography [7], and quantum communications systems [8]. Ideally, the quantum single-photon light source should emit strictly one photon at a time, where each photon is indistinguishable (cf. a train of photons), in a high repetition rate, thus functioning as a so called "photon gun."

There are several established schemes that can facilitate the emission of single photons [9]. The easiest and most straightforward way is to attenuate pulsed lasers [10], though in this case the production of single photons is probabilistic. Therefore, there may be no photons, several photons, or many photons, since the photon number generated is subject to Poissonian statistics; this can be problematic for a number of applications such as quantum cryptography because of possible photon number-splitting attacks ("eavesdropping") [11]. Recently there has been extensive research devoted to microscopic structures, where an isolated quantum system functions as a source for the emitted photons. In theory, a single quantum object behaving as a two-level system is an ideal single photon emitter, and there are many possible candidates that may show such behavior, including atoms [12], ions [13], molecules [14], and nitrogen vacancy centers [15]. In contrast to the low attenuated lasers and heralded schemes, the single photon emitter based on a single isolated quantum system can be deterministic and on demand, since a single two-level system can emit precisely one photon each time it is excited. Yet, many of these isolated quantum systems are impractical for a number of reasons, and can suffer from photo-bleaching and blinking, or have problems that stem from their broad optical spectrum, since the real systems are much more complicated than an idealized two-level system. From a practical perspective, semiconductor quantum dots (QDs) [1, 16, 17] offer an attractive material system for emitting single photons.

Owing to the great improvements in semiconductor fabrication technologies, many pioneering results in the synthesis and application of these powerful nanostructures have been demonstrated [1–18]. Quantum dots by molecular beam epitaxy prepared nanocrystals, also known as "artificial atoms" provide an ideal single-photon source for quantum cryptography and optical quantum computing. By virtue of their unique electronic structure and quantum confinement, single QD emitters reliably generate single photons on demand when excited by short optical or electrical pulses. There are some advantages about the QDs, such as large exciton dipole moments, integrity with compact semiconductor systems [17], fixed in position and stable, compatibility with electronics and lasers. Moreover, their excitonic emission spectra can be nano-engineered to cover ultraviolet, visible, and infrared frequencies, rendering them fully compatible with telecom sources and components. As a matter of fact, semiconductor colloidal QDs synthesized by wet chemical approaches as sources of single photons have been extensively studied in the past few years because of their low fabrication costs, high quantum efficiency and photostability also at room temperature [18]. Broad tunability of their emission wavelength from the visible to the infrared has been readily achieved by virtue of the high versatility in the chemical synthesis, which allows for excellent control over QDs size, shape and composition [19–21]. These colloidal nanocrystals (NCs) are good candidates for QDs photonic applications in different fields such as health, energy, environment and aerospace due to their low fabrication costs, high quantum efficiency at room temperature, high versatility in the chemical synthesis, and broad tunable emission range [24]. Moreover, recent years have seen an increasing use of semiconductor QDs or NCs as components of different nano-architectures of design due to their size dependent optical properties, which are culminating in the development of wet-chemistry syntheses of highly emissive monodisperse QDs with variable sizes and compositions. Their absorption and emission spectra are controlled both by chemical composition and by size because of the quantum confinement effect.

On the other hand, epitaxial QDs, obtained by the Stranski–Krastanov self-organized growth mode [22], have demonstrated their potential as light sources for ultrafast semiconductor lasers [5, 23–25] and optical amplifiers (SOAs) [26] for optical communications, showing new functionalities and astonishing performances such as high gain and efficiency, ultralow threshold current densities and temperature insensitivity. Both wet chemistry and epitaxy growth mode have demonstrated to be effective approaches for the fabrication of single QDs embedded in triggered non-classical sources of single photons. Notably, epitaxial QDs exhibit single photon emission only at cryogenic temperature [27], whereas single colloidal NCs based on II–VI compounds exhibit photon antibunching at room temperature and above [12, 28, 29], by virtue of their peculiar electronic properties.

In this work, recent developments on single photon sources based on single QDs are reviewed. We first recall quantum theory of QD-cavity system, and basic concepts related to the fluorescence and optical properties of colloidal NCs, with special emphasis on their photon antibunching, blinking and spectral diffusion phenomena.

In the third section we then discuss the technological approaches for isolating and positioning single colloidal QDs, an essential requirement for practical realization of single QD single photon sources. Then we report on the approaches to significantly enhance the emission efficiency of single photon sources by coupling the emission of single QDs to microcavity modes. The successful achievement of this challenging technological target leads to devices with enhanced performances in terms of extraction efficiency, low divergence and improved emission efficiency in both weak and strong coupling regimes. We will discuss the recent progress in the fabrication of single photon sources, and various approaches for embedding single QDs into microcavities or photonic crystal nanocavities, and show how to extend the wavelength range. We focus in particular on new generations of electrically driven QD single photon source leading to ultralow pump currents, high repetition rates, and high collection efficiencies at elevated temperature operation. Electrically driven triggered sources of single photons are highly attractive since they would bring compact SPSs to practical application without requiring expensive and sizeable light excitation sources. Besides, new developments of room temperature single photon emission in the strong coupling regime are reviewed. Finally, the generation of indistinguishable photons and remaining challenges for practical single-photon sources are also discussed.

2 Theory, model and measurement aspects

2.1 Theory of quantum optics and photon statistics

QDs referred to as artificial atoms usually contain several hundred thousands of atoms, but nevertheless have energy levels that mimic the behavior of a two-level system. However, the observed flopping behavior is heavily damped, since semiconductor QDs suffer from the usual solid-state problems of environment-induced decoherence [30, 31]. Decoherence has a major influence in the indistinguishable nature of the emitted photons, and is one of the biggest obstacles in realizing quantum information processing. Thus, most experiments performed to date work at cryogenic temperatures (∼4 K is typical), yet this alone is not enough to overcome the problems of decoherence. As a result, one must somehow have the photon emitted fast enough (before the onset of decoherence becomes significant), which can be achieved by engineering the surrounding photon density of states that the QD sees. In this regard, it is now known that spontaneous emission of an atom or QD (photon emitter) can be strongly modified by the external dielectric environment due to the Purcell effect [32], which is an example of cavity-quantum electrodynamics (cavity-QED). This is precisely why the microcavities and inhomogeneous material systems are so important.

The quantum properties of the photon emitted from semiconductor microcavities containing QDs have gained considerable interest both for fundamental aspects [1–5] and for potential applications [2, 4, 6], such as single photon sources. Strong coupling occurs when the square of emitter–photon interaction becomes larger than the combined atomic dipole decay rate and the cavity field decay rate. The regime of strong coupling between a single exciton confined in a QD has been achieved in microcavity systems based on microdiscs [2], in photonic crystal nanocavities [3] and in pillar microcavities [4, 33]. In all these structures, quantum electrodynamics (QED) effects of zero-dimensional electron systems interacting with optical modes, like the Purcell effect or Rabi splitting, have been observed [1–5, 25].

In this section, the prerequisite formalism for the theoretical description of the quantum optics and photon statistics on the two-level quantum emitter-cavity system for single photon sources is briefly presented here for completeness. A more general and detailed theoretical formalism and discussion can be found in Refs. [34, 35].

• Theory for quantum emitter decay via a cavity

A two-level QD emitter in its excited state decays in a finite Q single-mode microcavity. After waiting long enough, a single photon will be found in either of the two radiation continuum: the α-continuum representing the radiation of the cavity mode or the β-continuum representing the radiation through leaky modes. We want to know what part of the light actually decays through the cavity and determines its spectrum. As shown in Fig. 1, a two-level QD emitter with energy separation ω_0 and dipole moment μ is coupled to a single cavity resonant mode of ω_c. And the cavity mode with normalized electric field and creation operator is coupled to a radiation continuum labeled by index α with coupling constants C_α and dispersion $\omega(\alpha)$. The emitter also has the possibility to decay directly in the environment, modeled as a radiation continuum with coupling constants D_β and dispersion $\omega(\beta)$. We assume that the α and β continua are orthogonal, so that they do not interact with each other. We use the Wigner–Weisskopf approximation to define the spontaneous emission rate of the two-level system into the β-continuum as γ and the energy decay rate of the cavity mode into the α-continuum as κ. Using the Wigner–Weisskopf approximation, we have

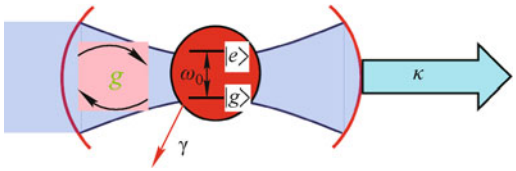

Fig. 1 A two-level QD emitter with energy separation ω_0 and dipole moment μ is coupled to a single cavity mode resonant radiation modes of ω_c. γ is the spontaneous emission rate of the two-level system into the β-continuum and κ is the energy decay rate of the cavity mode into the α-continuum.

$$\kappa = 2\pi \int \mathrm{d}\beta |C_\alpha|^2 \delta(\omega(\alpha) - \omega) \tag{1}$$

$$\gamma = 2\pi \int \mathrm{d}\beta |D_\beta|^2 \delta(\omega(\beta) - \omega) \tag{2}$$

Note that γ can differ from the free space spontaneous emission rate because the cavity changes the structure of the vacuum around the emitter. The cavity mode electric field is denoted by

$$\hat{E}_c(r) = \mathrm{i}\frac{\bar{E}_c(r)}{\sqrt{\max \varepsilon(r)|\bar{E}_c(r)|^2}}\sqrt{\frac{\hbar\omega_c}{2\varepsilon_0 V_m}}a_c + h.c. \tag{3}$$

where the cavity field mode amplitude can be normalized so that

$$\int \mathrm{d}^3 r \varepsilon(r)|\bar{E}_c(r)|^2 = 1 \tag{4}$$

$\bar{E}_c(r)$ is the normalized cavity field profile, and a_c and a_c^+ is the corresponding annihilation and creation operator, respectively. Now we use the coupled mode theory between the single photon states to further understand the underlying properties of the present device. The quantum emitter's coupling constant to the empty cavity mode in the Jaynes–Cummings is

$$g = \mathrm{i}\frac{\mu^* \cdot \bar{E}_c(r)}{\hbar} = \mathrm{i}\sqrt{\frac{\omega_c}{2\hbar\varepsilon_0 V_m}}\frac{\mu^* \cdot \bar{E}_c(r)}{\sqrt{\max \varepsilon(r)|\bar{E}_c(r)|^2}} \tag{5}$$

If we assume that the QD resonantly couples with the cavity mode, the interaction Hamiltonian in the rotating-wave approximation can be written as

$$H_I = \mathrm{i}g|e\rangle\langle g|a_c + h.c. \tag{6}$$

We assume that the two-level quantum dot emitter is prepared in its excited state and that the radiation continuum starts off in their vacuum state. The state of the system can be given at all times by [35, 36]

$$|\Psi(t)\rangle = a(t)|e, 0_c, 0_\alpha, 0_\beta\rangle + b(t)|g, 1_c, 0_\alpha, 0_\beta\rangle + \sum_\alpha c_\alpha(t)|g, 0_c, 1_\alpha, 0_\beta\rangle + \sum_\beta d_\beta(t)|g, 0_c, 0_\alpha, 1_\beta\rangle \tag{7}$$

According to the Schrodinger equation, we have

$$\frac{\mathrm{d}a}{\mathrm{d}t} = -\mathrm{i}g\mathrm{e}^{\mathrm{i}(\omega_0-\omega_c)t}b - \mathrm{i}\sum_\beta D_\beta \mathrm{e}^{\mathrm{i}(\omega_0-\omega_\beta)t}d_\beta \tag{8}$$

$$\frac{\mathrm{d}b}{\mathrm{d}t} = -\mathrm{i}g^*\mathrm{e}^{-\mathrm{i}(\omega_0-\omega_c)t}a - \mathrm{i}\sum_\alpha C_\alpha \mathrm{e}^{\mathrm{i}(\omega_0-\omega_\alpha)t}c_\alpha \tag{9}$$

$$\frac{\mathrm{d}c_\alpha}{\mathrm{d}t} = -\mathrm{i}C_\alpha^*\mathrm{e}^{\mathrm{i}(\omega_\alpha-\omega_c)t}b \tag{10}$$

$$\frac{\mathrm{d}d_\beta}{\mathrm{d}t} = -\mathrm{i}D_\beta^*\mathrm{e}^{\mathrm{i}(\omega_\beta-\omega_0)t}a \tag{11}$$

with initial conditions:

$$a(0) = 1 \tag{12}$$

$$b(0) = c_\alpha(0) = d_\beta(0) = 0 \tag{13}$$

Using Laplace transforms, we solve those equations and obtain

$$s\bar{a}(s) - 1 = -\mathrm{i}g\bar{b}[s - \mathrm{i}(\omega_0 - \omega_c)] - \mathrm{i}\sum_\beta D_\beta \bar{d}_\beta[s - \mathrm{i}(\omega_0 - \omega_\beta)] \tag{14}$$

$$s\bar{b}(s) - 1 = -\mathrm{i}g^*\bar{a}[s + \mathrm{i}(\omega_0 - \omega_c)] - \mathrm{i}\sum_\alpha C_\alpha \bar{c}_\alpha[s - \mathrm{i}(\omega_c - \omega_\alpha)] \tag{15}$$

$$s\bar{c}_\alpha(s) = -\mathrm{i}C_\alpha^*\bar{b}[s - \mathrm{i}(\omega_\alpha - \omega_c)] \tag{16}$$

$$s\bar{d}_\beta(s) = -\mathrm{i}D_\beta^*\bar{a}[s - \mathrm{i}(\omega_\beta - \omega_0)] \tag{17}$$

From this set of equations above, we obtain

$$\bar{a}(s) = \left[s + \frac{g^2}{s - \mathrm{i}(\omega_0 - \omega_c) + \sum_\alpha \frac{|C_\alpha|^2}{s - \mathrm{i}(\omega_0 - \omega_\alpha)}} + \sum_\beta \frac{|D_\beta|^2}{s - \mathrm{i}(\omega_0 - \omega_\beta)}\right]^{-1} \tag{18}$$

$$\bar{b}(s) = -\mathrm{i}g^*\frac{\bar{a}(s + \mathrm{i}(\omega_0 - \omega_c))}{s + \sum_\alpha \frac{|C_\alpha|^2}{s + \mathrm{i}(\omega_\alpha - \omega_c)}} \tag{19}$$

$$\bar{c}_\alpha(s) = -\mathrm{i}C_\alpha^*\frac{\bar{b}(s - \mathrm{i}(\omega_\alpha - \omega_c))}{s} \tag{20}$$

$$\bar{d}_\beta(s) = -\mathrm{i}D_\beta^*\frac{\bar{a}(s - \mathrm{i}(\omega_\beta - \omega_0))}{s} \tag{21}$$

The function $\bar{c}_\alpha(s)$ has three poles, though two of them have a strictly negative real part and hence contribute only to the transient temporal behavior. The asymptotic population of the α-continuum is described by the $s = 0$ pole of $\bar{c}_\alpha(s)$:

$$c_\alpha(t \to \infty) = \lim_{s\to 0^+} -\mathrm{i}C_\alpha^*\bar{b}[s - \mathrm{i}(\omega_\alpha - \omega_c)] \tag{22}$$

To perform this limit, using the relation from distribution theory, we obtain the results:

$$\lim_{s\to 0^+}\sum_{\alpha}\frac{|C_\alpha|^2}{s-\mathrm{i}(\omega_0-\omega_\alpha)}=\frac{\kappa}{2}+\mathrm{i}\delta_a \tag{23}$$

And similarly,

$$\lim_{s\to 0^+}\sum_{\beta}\frac{|D_\beta|^2}{s-\mathrm{i}(\omega_0-\omega_\beta)}=\frac{\gamma}{2}+\mathrm{i}\delta_b \tag{24}$$

The terms arising from the principal part integrals represent the Lamb Shift or energy renormalization of the quantum emitter due to its coupling to the α-continuum and β-continuum respectively, which can be usually omitted for simplicity.

The asymptotic amplitudes of the states in the α-continuum are then given by

$$\begin{aligned}&c_\alpha(t\to\infty)\\&=C_\alpha\frac{g_0}{\left(\omega_\alpha-\omega_c+\mathrm{i}\frac{\kappa}{2}\right)\left(\omega_\alpha-\omega_0+\mathrm{i}\frac{\gamma}{2}\right)-|g_0|^2}\end{aligned} \tag{25}$$

The corresponding probability distribution is $|C_\alpha|^2$. The asymptotic amplitudes of the leaky mode states in the β-continuum are

$$\begin{aligned}&d_\beta(t\to\infty)\\&=D_\beta\frac{\omega_\beta-\omega_c+\mathrm{i}\frac{\kappa}{2}}{\left(\omega_\beta-\omega_c+\mathrm{i}\frac{\kappa}{2}\right)\left(\omega_\beta-\omega_0+\mathrm{i}\frac{\gamma}{2}\right)-|g_0|^2}\end{aligned} \tag{26}$$

Next, we can compute the total probability of the quantum emitter decay into the α-continuum:

$$\begin{aligned}P_{\text{cavity}}&=\sum_\alpha|c_\alpha(t\to\infty)|^2\\&=\int\mathrm{d}\omega\left[\int\mathrm{d}\alpha|c_\alpha(t\to\infty)|^2\delta(\omega-\omega_\alpha)\right]\\&=|g|^2\frac{\kappa}{2\pi}\int\frac{\mathrm{d}\omega}{(\omega-\omega_1)(\omega-\omega_1^*)(\omega-\omega_2)(\omega-\omega_2^*)}\\&=\frac{|g|^2\kappa}{|\omega-\omega_2^*|^2}\left|\frac{1}{\mathrm{Im}(\omega_1)}+\frac{1}{\mathrm{Im}(\omega_2)}\right|\\&=\frac{|g|^2\kappa}{|\omega-\omega_2^*|^2}\left|\frac{\mathrm{Im}(\omega_1+\omega_2)}{\mathrm{Im}(\omega_1)\mathrm{Im}(\omega_2)}\right|\\&=\frac{|g|^2\kappa(\kappa+\gamma)}{\kappa\gamma\left(\Delta^2+\frac{(\kappa+\gamma)^2}{4}\right)+(\kappa+\gamma)^2|g|^2}\\&=\frac{\kappa}{\kappa+\gamma}\frac{F_p}{F_p+1+\frac{4\Delta^2}{(\kappa+\gamma)^2}}\end{aligned} \tag{27}$$

where ω and ω are the poles of the $c\alpha$ function of ω. $\Delta=\omega_0-\omega_c$ are the detuning frequency of the quantum emitter with respect to the cavity resonance. And F_p is the so-called Purcell factor written as

$$F_p=\frac{4|g|^2}{\kappa\gamma} \tag{28}$$

In particular, when the quantum emitter's frequency is resonant with the cavity mode, the emission in the cavity is the maximum and is given by

$$P_{\text{cavity}}=\frac{\kappa}{\kappa+\gamma}\cdot\frac{F_p}{F_p+1} \tag{29}$$

The coupling of the cavity mode to radiation modes can be modeled with an effective Hamiltonian:

$$H_{\text{int}}^{C-R}=\hbar\int\mathrm{d}\beta\frac{\mu\cdot\bar{E}_c(r)}{\hbar}c^+a_\beta+h.c. \tag{30}$$

Using the Laplace transformation, we can obtain the output amplitude of the emitted single photon has an oscillatory nature given explicitly by

$$\alpha^{\text{out}}(\tau)=\mathrm{i}g\sqrt{\kappa}\frac{\mathrm{e}^{-\frac{\kappa+\gamma}{4}t}\sin\sqrt{|g|^2-\left(\frac{\kappa-\gamma}{4}\right)^2}t}{\sqrt{|g|^2-\left(\frac{\kappa-\gamma}{4}\right)^2}} \tag{31}$$

whereas in the weak coupling regime, it is purely bi-exponential

$$\alpha^{\text{out}}(\tau)=\mathrm{i}g\sqrt{\kappa}\frac{\mathrm{e}^{-\frac{\kappa+\gamma}{4}t}\sinh\sqrt{\left(\frac{\kappa-\gamma}{4}\right)^2-|g|^2}t}{\sqrt{\left(\frac{\kappa-\gamma}{4}\right)^2-|g|^2}} \tag{32}$$

In most uses of single-photon sources, the useful light is the fraction collected in the cavity radiation modes. Thus, the efficiency to collect a single photon for such a device is

$$\eta_{\text{cavity}}\approx\frac{F_p}{F_p+1}\cdot\frac{\kappa}{\kappa+\gamma} \tag{33}$$

where the first term represents the loss through spontaneous emission directly into leaky modes outside of the cavity, and the second term represents the loss of the cavity photon to modes other than the desired one. The most efficient configuration to extract the light through the cavity is to have $\frac{\kappa}{2}=g$, in which case the extracted light fraction is

$$\eta_{\text{cavity}}^{\max}=\left(1+\frac{\gamma}{2g}\right)^{-2} \tag{34}$$

At this point, we can conclude that the achievable maximum of the total efficiency of such an electrically driven single-QD-cavity, a single photon source device, is determined by the spontaneous emission rate of the QD emitter itself. Fortunately, through precise fabrication of different kinds of QDs, we have a rather wide choice of selecting some QD to achieve the maximal efficiency.

2.2 Classification of light states and photon statistics

In order to better understand the features of a single-photon source it is instructive to compare first the statistical properties of thermal light and coherent light.

• Thermal, coherent and photon number states

Different light fields can be characterized by their specific photon number fluctuations. Thermal radiation results from a thermal equilibrium of emission and absorption between a radiation field and an ensemble of emitters (e.g., atoms in a discharge lamp). In such a system the photon number probability distribution can be written in terms of the mean photon number $\langle n\rangle$ as the geometric distribution [35, 36]

$$P(n) = \frac{\langle n\rangle^n}{(1+\langle n\rangle)^{1+n}} \tag{35}$$

It can be found that $n = 0$ has always the largest probability and the distribution falls off monotonically with increasing n. As shown in Fig. 2(a), the photon number fluctuations are expressed in statistical terms by the variance of the distribution $(\Delta n)^2 = \langle n^2\rangle - \langle n\rangle^2$. For a thermal mode, the variance is found to be $(\Delta n)^2 = \langle n\rangle^2 + \langle n\rangle$ [35].

The coherent state (*Glauber* state) is characterized by the minimum uncertainty product [36] in accordance with the Heisenberg uncertainty relation for energy and time. An example for a coherent light source is a laser which is operated well above the threshold. The photon number distribution in this state is a Poisson distribution, i.e., the probability to find n photons in the coherent state with respect to the mean photon number is given by

$$P(n) = \mathrm{e}^{-\langle n\rangle}\frac{\langle n\rangle^n}{n!} \tag{36}$$

Poisson distributions are shown in Fig. 2(b) for two mean photon numbers n and they are peaked at the mean photon numbers, respectively. The variance is calculated to $(\Delta n)^2 = \langle n\rangle$ [2]. Whereas for thermal radiation the fluctuations are always comparable with the mean photon number in the mode, and the relative fluctuations $(\Delta n/\langle n\rangle = 1/\sqrt{\langle n\rangle})$ for coherent light approach zero with increasing photon numbers. Therefore, the coherent light best approaches the pure classical picture of waves with fully determined amplitude and phase, i.e., revealing zero uncertainties. It is obvious from Fig. 2 that single photons on demand cannot be generated by simply attenuating a light beam steaming from a thermal or a coherent light source. Such a nonclassical light state can only be generated by a single-photon source as will be shown below.

A photon number or a Fock state $|n\rangle$ is a truly nonclassical light state. It can be generated by a single-photon source. The Fock state is the eigenstate of the photon number operator: $\hat{n}|n\rangle = n|n\rangle$, i.e., a mode which is excited in this state is occupied by exactly n photons and the variance $\Delta n = 0$. Figure 2(c) illustrates the photon number distributions for the Fock states with nonzero probability given exclusively for the mean photon number $\langle n\rangle = n$.

2.3 Photon detection and correlation functions

This section introduces the prerequisite formalism for the

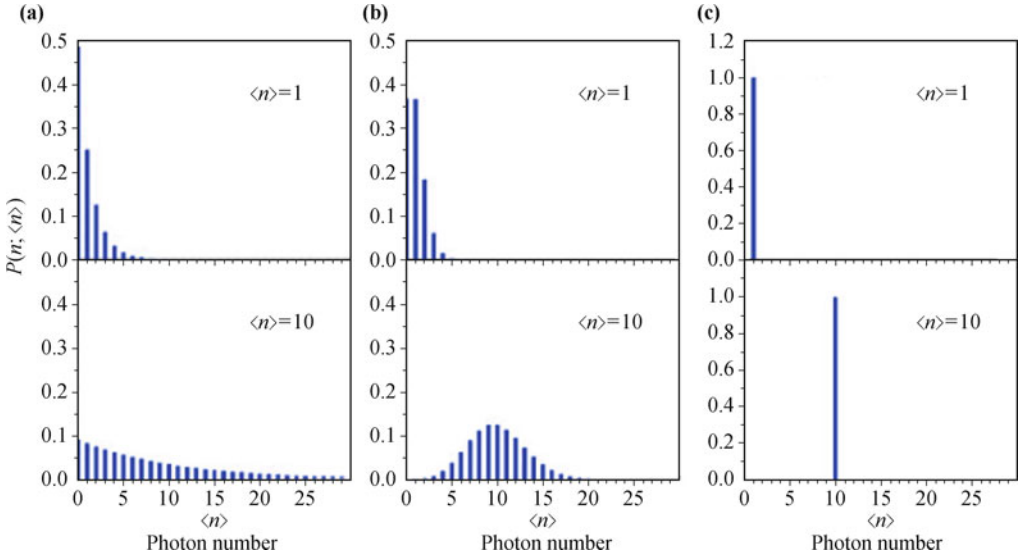

Fig. 2 Photon number probability distribution for single mode emission of **(a)** a thermal state, **(b)** a coherent state, and **(c)** a photon number state for two different mean photon numbers $\langle n\rangle = 1$, 10, respectively.

theoretical description of the experimental results on the coherence and photon statistics of the light sources. A more general, detailed and careful discussion can be found in Refs. [4, 34–37].

Photons are typically detected by photodetectors or avalanche photodiodes. In this case the photon is absorbed and as a consequence the quantum state of the light field is altered. The probability of photon detection P_1, which is associated with a transition from an initial field state Ψ_i to possible final states Ψ_f via absorption of a photon, is given by

$$P_1(t) \sim \sum_f |\langle\psi_f|\hat{a}(t)|\psi_i\rangle|^2 \sim \langle\psi|\hat{a}^+(t)\hat{a}(t)|\psi\rangle \tag{37}$$

where the sum goes over all possible final states and $\hat{a}(t)$ denotes the photon destruction operator in the Heisenberg picture. The *first-order coherence* function is defined as

$$g^{(1)}(\tau) = \lim_{t\to\infty} \frac{\langle\hat{a}^+(t)\hat{a}(t+\tau)\rangle}{\langle\hat{a}^+(t)\hat{a}(t)\rangle} \tag{38}$$

and the corresponding degree of *second-order coherence* is defined by

$$g^{(2)}(\tau) = \lim_{t\to\infty} \frac{\langle\hat{a}^+(t)\hat{a}^+(t+\tau)\hat{a}(t+\tau)\hat{a}(t)\rangle}{\langle\hat{a}^+(t)\hat{a}(t)\rangle^2} \tag{39}$$

The first and second order coherence functions are commonly measured by a *Michelson interferometer* and a *Hanbury–Brown and Twiss* setup, respectively. When the light is stationary, only the relative time $\tau = t_2 - t_1$ is relevant. It is found that the photon detection probability, i.e., the counting rate of the photodetector is in fact just the first-order correlation function except for a scale factor. Furthermore, the first-order correlation is insensitive to the photon statistics since Eq. (38) depends only on the average photon number $\langle n\rangle = \langle\hat{a}^+(t)\hat{a}(t)\rangle$. In other words, spectrally-filtered thermal light and coherent light of the same spectral width exhibit the same degree of first-order coherence. In contrast, the second-order correlation function allows for distinguishing between the different types of light fields. It is interesting to compare $g^{(2)}(0)$ for thermal, coherent, and photon number states:

(i) Coherent light

$$g^{(2)}(0) = \frac{\langle\alpha|\hat{a}^+\hat{a}^+\hat{a}\hat{a}|\alpha\rangle}{\langle\alpha|\hat{a}^+\hat{a}|\alpha\rangle^2} = 1 \tag{40}$$

(ii) Photon number states

$$g^{(2)}(0) = \frac{\langle n|\hat{a}^+\hat{a}^+\hat{a}\hat{a}|n\rangle}{\langle n|\hat{a}^+\hat{a}|n\rangle^2} = 1 - \frac{1}{n} \tag{41}$$

This is a truly nonclassical result since $g^{(2)}(0) < 1$ for $n \geqslant 1$. The light is called to be in a *sub-Poissonian* light state. Especially, for a true single-photon source ($n = 1$) $g^{(2)}(0) = 0$.

(iii) Thermal light

$$g^{(2)}(0) = 1 + \frac{(\Delta n)^2 - \langle n\rangle}{\langle n\rangle^2} = 2 \tag{42}$$

This indicates that photons have the tendency to be detected simultaneously at the photodetectors. The light is called to be in a *super-Poissonian* light state.

The detailed theory and calculation of the photon correlation function $g^{(2)}(\tau)$ as a function of the delay time τ can be found in Refs. [2, 34]. For a coherent source $g^{(2)}(\tau) = 1$, which means that the photons are completely uncorrelated. In contrast, a sub-Poissonian light source satisfies $g^{(2)}(\tau) < 1$, which indicates that two photons are unlikely to be detected simultaneously by the detectors. A light emission from a single quantum emitter, whose degree of second-order coherence satisfies the inequality $[g^{(2)}(0) \leqslant g^{(2)}(\tau)]$ is called antibunched light (*photon antibunching*). On the other hand, a light source with a super-Poissonian statistics shows a clear excess of coincidences $[1 < g^{(2)}(\tau) < 2]$ for times shorter than the coherence time T_2 of the light source. This phenomenon $[g^{(2)}(\tau) \leqslant g^{(2)}(0)]$ is called *photon bunching*.

2.4 Measurement of the second-order correlation function

Experimentally, there are different experimental techniques that can be used to measure the second-order correlation function $g^{(2)}(\tau)$. The most popular and direct method would be to measure the times of a single-photon detector's counting events to calculate the correlation function. However, this method has a measurement limit that the time scales would be longer than the dead time of the detector, which amounts to several 10 ns. In order to overcome this problem, detection schemes using two independent detectors with the time-correlated single photon counter (TCSPC) modules in a Hanbury–Brown–Twiss scheme setup shown in Fig. 3 are usually employed. The setup consists of two orthogonally arranged pathways centered around a non-polarizing (50/50) beam splitter. Each arm of the HBT interferometer is equipped with a highly sensitive single photon detector. In such an arrangement, the second detector can detect an event while the first one is still dead, and the time-resolution is typically determined by the response time of the detector. Presently, the commercial avalanche photodetector modules (APDs), which offer the highest detection efficiencies (~40%–70%) in the visible and near infrared spectrum, have response times of about 400–600 ps. APDs with slightly lower detection

efficiencies (∼5%–35%) possess response times in the 30–50 ps range.

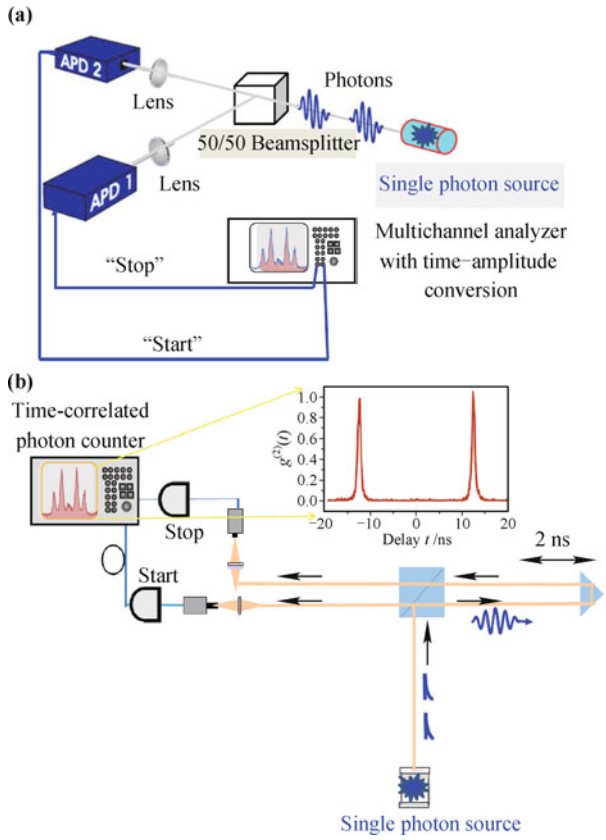

Fig. 3 Photon autocorrelation setup after Hanbury–Brown and Twiss. **(a)** The collected photon stream from a single photon source is prefiltered by a spectrometer (alternatively: narrow band filters) and sent to fast avalanche photodetectors (APDs) through a 50/50 nonpolarizing beamsplitter (NPBS). The photon coincidence statistics $n(\tau)$ are measured by combined time-amplitude conversion (TAC) and multichannel analysis (MCA). **(b)** Scheme of the Hanbury Brown–Twiss setup. The photon coincidence statistics $n(\tau)$ are measured by combined time-correlated photon counter with correlation measurement of a spectral line of a single QD.

Technically, two operation methods can be distinguished. In the first approach shown in Fig. 3(a), a time-tagged method for the recording of individual photon events with their arrival time on both channels is used. This allows the most flexible offline analysis of the photon dynamics. Drawbacks are large data sets and the fact that the computation of the correlation function is very time consuming. In the second method shown in Fig. 3(b), only the time differences between the detection events (Start and Stop) are registered and in a subsequent process a time to-amplitude conversion followed by a multichannel analysis is performed in order to generate a histogram of coincidence events $n(\tau)$. One has to consider that the measured coincidence function $n(\tau)$ differs from the original second order coherence function $g^{(2)}(\tau)$. The probability to measure a time difference at time τ is given by [35, 37]:

$n(\tau)$ = (probability to measure a stop event at time τ after a start event at time 0) × (probability that no stop detection has occurred before)

$$n(\tau) = [G^{(2)}(\tau) + R_{\mathrm{dark}}][1 - \int_0^{\tau} n(\tau')\mathrm{d}\tau'] \qquad (43)$$

where $G^{(2)}(\tau)$ is the unnormalized second-order coherence function and R_{dark} describes the detector dark counts. The measured histogram of coincidence counts $n(\tau)$ approaches $G^{(2)}(\tau)$ in the limit when R_{dark} is much smaller than the signal count rate R, and the average arrival time of the photons $1/R$ is much smaller than the observed delay time τ. This means that the probability that no stop detection has occurred before is approximately 1. Losses, like undetected photons, lead only to a global decrease of $G^{(2)}(\tau)$ which can be compensated, e.g., with a longer measuring time. An exact solution of the above integral equation shows that $n(\tau)$ exhibits an exponential decrease on a time scale given by the detector count rate [37]. It should be noted that interest has been intensified in recent years in such a fluorescence correlation spectroscopy detection schemes using two independent detectors with the time-correlated single photon counter (TCSPC) modules in a Hanbury–Brown–Twiss scheme setup to monitor the complex bio- or nano-conjugates at single-molecule level [38].

Most of the photon antibunching reported on QDs in the literature are II-VI colloidal NCs with a CdSe spherical core embedded in either CdS or ZnS shells. In 2009, Qualtieri *et al.* [39] showed for the first time the occurrence of photon antibunching at room temperature from single colloidal CdSe/ZnS NCs inserted in an ordered array of vertical microcavities. The approach relies on the single NC localization technique obtained by direct electron beam lithography sandwiched between SiO_2/TiO_2 Bragg mirrors consisting of four alternating quarter-wavelength thick layers of TiO_2/SiO_2 [39]. In CdSe/CdS NCs, by virtue of a low lattice mismatch, the influence of defects on the radiative recombination process is reduced, as well as the influence of surface traps on single excitons, which usually tend to increase the average radiative lifetime of the system. The full control on the growth parameters in the wet chemical synthesis process was exploited to synthesize different NCs such as rods, dot in rods, tetrapods and also dimers [19, 21, 40–43]. Most of these NCs demonstrated to be effective sources of single photons. In particular nanorods, i.e., elongated NCs, and CdSe/CdS QD-in-rods, obtained by surrounding a spherical CdSe core with an elongated CdS shell [21, 41], appear to be very promising quantum

emitters by virtue of their relatively short lifetime and electrical dipole-moment oriented along the rod axis [21, 41], which leads to a higher degree of linear polarization [19, 41]. Here it should be pointed out that typical NCs are nanometer-sized spherical core-shell structures, and the role of the shell is to engineer the band structure of the nanostructure and to passivate the core surface, thus reducing the surface defects, such as dangling bonds, which dramatically affect their efficiency and photostability. Figure 4 shows the single nanoparticle photoluminescence spectra of a single core-shell CdSe/CdS nanorod with correlation measurement. This invaluable feature enables a deterministic photon polarization to be achieved for a single photon source device, as required in BB84 and B92 cryptographic algorithms [44]. Besides, De Vittorio *et al.* [45] have shown that the polarization control of single photons can be achieved by using QD-in-rods rotated at different angles, envisioning a strategy to develop polarization controlled and highly efficient room temperature single photon sources. On the other hand, most of the photon antibunching reported on QDs are InGaAs or InP/GaInP QDs on GaAs substrate grown by molecular beam epitaxy (MBE) [2–4, 23, 46]. The most established method for preparing such QDs is the self-assembled Stranski–Krastanov growth mode [46, 47], which produces nanostructures with very high crystal quality and quantum efficiencies close to unity. The QDs, which are very promising single-photon emitters for quantum communication systems, appear spontaneously due to lattice mismatch during MBE growth.

3 Fluorescence and excition properties of single quantum dots

3.1 Fluorescence properties of single quantum dots

As mentioned before, typical NCs are nanometer-sized spherical core-shell structures, and the role of the shell is to engineer the band structure of the nanostructure and to passivate the core surface, thus reducing the surface defects, such as dangling bonds, which dramatically affect their efficiency and photostability. In particular, one strategy to control and completely prevent blinking proposed by Mahler and co-workers has shown that a thicker shell in CdSe–CdS NCs allows one to control the blinking behavior [48], suggesting that well-designed shells are the key parameters for obtaining non-blinking QDs. Due to their absorption continuum at energies above the exciton transition, they can be excited by a variety of light sources. Moreover, QDs combine atom-like properties such as a discrete energy spectrum and sharp lines in photoluminescence with the advantage that their emission wavelengths can be tailored to a large extend. Although the electronic shell structure, the spin structure, and the many-body interactions between electrons and holes usually have to be considered, in careful experimental conditions recombination from higher excited states, multi-exciton and charged excitons is typically negligible because of strong Auger processes [49], and the emission of single photons can be made highly probable only from single exciton recombination. In spite of their excellent quantum efficiency and photostability, colloidal QDs, when observed at the single particle level, exhibit fluorescence blinking and spectral diffusion. The first effect consists of the random switching of fluorescence between bright ("on") and dark ("off") states [50]. Such a fluctuation of the luminescence over time has been attributed to charge transfer or charge escape from the QD, which leads to a free charge in the QD, preventing any possible radiative recombination for times in the order of milliseconds. Besides, non-blinking behaviour has also been obtained in ternary CdZnSe/ZnSe NCs, designed as a radial graded alloy of CdZnSe into ZnSe [51].

Spectral diffusion consists of random spectral jumps ascribed to charge movements or, more generally, instability in the nanoscale environment of the NCs, which cause strong fluctuations of local electric fields [52, 53]. The resulting linewidth of single NCs is broadened by the time integration of NCs emission at slightly shifted wavelengths. In CdSe/ZnS single colloidal NCs, a spectral diffusion of 4 μeV over a time scale of 200 μs was observed for an emission peak having a linewidth as narrow as 6.5 μeV [54]. In the past few years, the excellent emission efficiency at room temperature, good stability and advances in high spatial resolution spectroscopic techniques has allowed a deeper understanding of the peculiar optical properties of QDs by probing QDs at single particle level [21, 50, 52]. Recent advances of efficient single photon emission at room temperature corroborate the potential of these nanostructures as active medium of single photon sources.

3.2 Exciton properties of QDs

High-quality self-assembled QDs can be grown by epitaxy growth techniques, in which strain induced islands are used to form self-assembled QDs. Important properties of a perfect single photon source are good optical spectra or exciton properties, an internal quantum efficiency of unity, a predetermined photon emission time (no jitter), and the indistinguishability of the emitted photons. In order to understand their detailed optical spectra, the electronic shell structure, the spin structure,

and the many-body interactions between electrons and holes have to be considered [55–57]. For an even number of electron and holes in a QD, one can observe the neutral complexes form, and relying on the population, one can observe the recombination from, e.g., the exciton (one electron, one hole), the biexciton (two electrons, two holes) and multiexcitonic (N electrons, N holes) states. For an odd number of particles in the QD, charged exciton transitions take place. Due to the Coulomb correlations between the carriers all transitions possess distinct and somewhat different energies. Therefore, they can all be used in principle as an emitter for single photon source by spectral filtering provided some restrictions are fulfilled. However, the biexcitonic or the excitonic transitions have been used in most demonstrations, in which a distinct fine-structure occurs in their emission spectra which can be understood if the spin structure of electrons and holes are considered.

The projection of the electronic spin on the z-axis (growth axis) of the QD is either $1/2$ or $-1/2$, whereas the heavy-hole spin projection is either $3/2$ or $-3/2$. This results in four distinct spin values for one electron–hole pair (exciton) in the QD. The two bright states $|-\frac{1}{2},\frac{3}{2}\rangle$ and $|\frac{1}{2},-\frac{3}{2}\rangle$ have a total z-spin of ±1 and are coupled to the light field, whereas the other two states $|\frac{1}{2},\frac{3}{2}\rangle$ and $|-\frac{1}{2},-\frac{3}{2}\rangle$ have a total z-spin of ±2 and are therefore optically decoupled, i.e., dark, due to the selection rules for dipole transitions. In the idealized case where the QD possesses a perfect cylindrical symmetry around its growth axis, the $\pm|1\rangle$ states are degenerate. Yet, in practice most of the QDs are asymmetric; as a result, the degeneracy is lifted by the electron–hole exchange interaction resulting in a doublet structure shown in Fig. 5. For example, this fine structure splitting for InGaAs/GaAs is in the range of ∼0–100 μeV. Thus, the excitonic recombination line is split in energy and the individual components possess orthogonal linear polarizations [55]. Typically, one of the linear polarizations is aligned with one of the substrates cleave directions (i.e., for GaAs (110) or (1–10)).

The biexciton is a spin-singlet state which does not reveal a fine structure itself but decays to one of the two optically bright excitonic states. The simplest charged excitonic configuration (trion $X_{\pm}$) is given by one s-shell exciton plus a single excess carrier (electron or hole). Exemplarily, for the negatively charged trion complex X_{-} the two s-electrons must have opposite spins due to the Pauli exclusion principle, whereas both spin orientations are allowed for the hole. As a consequence, there is no fine structure splitting.

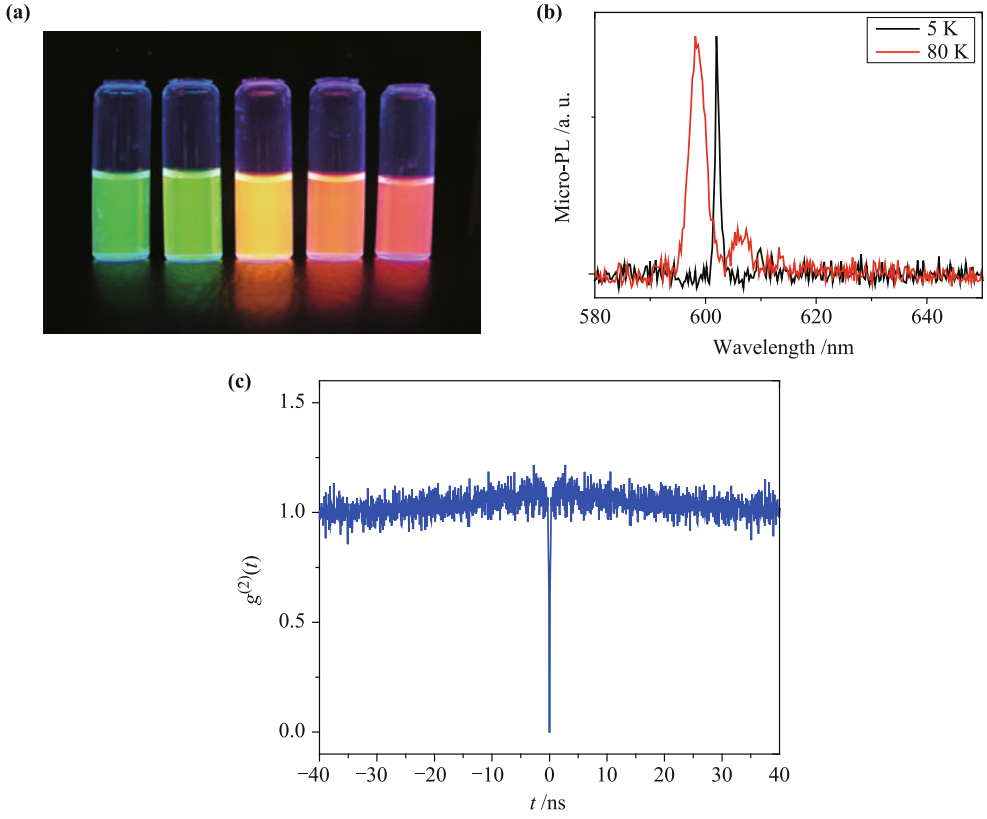

Fig. 4 **(a)** Different high-bright colors of monodispersive CdSe/CdS core-shell NCs with high quality by program process of microwave irradiation. **(b)** Single nanoparticle photoluminescence spectra of a single CdSe/CdS NC with second-order correlation measurement **(c)**.

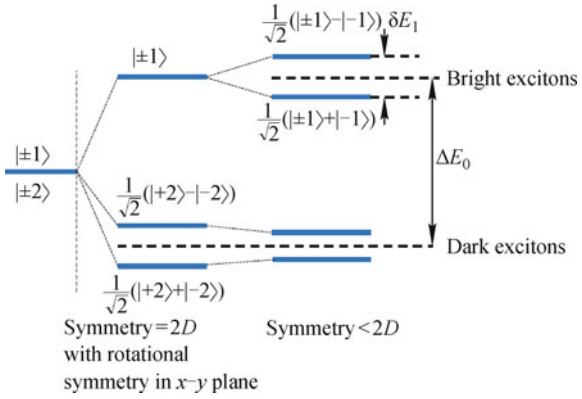

Fig. 5 Energy level scheme for the excitonic QD ground state without and with inclusion of exchange interaction between electron and hole spins. The initial fourfold exciton degeneracy for non-interacting spins is lifted thus forming optically allowed "bright" and forbidden "dark" configurations. The bright states are further split into a doublet under the conditions of lowered in-plane symmetry.

In practice, the properties like internal quantum efficiency, jitter, coherence time, polarization of the emitted single photons critically depend on the excitation process. As shown in Fig. 6, there are totally three main excitation schemes for the realization of single-photon sources.

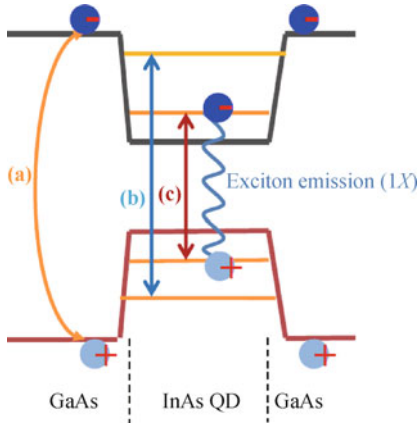

Fig. 6 Three main excitation schemes **(a)** Non-resonant, **(b)** quasi-resonant, and **(c)** resonant optical excitation schemes.

In the case of non-resonant excitation, after pulsed excitation of the QD above the barrier bandgap the electron–hole pairs are mainly generated in the barrier and subsequently electron and holes are captured by the QDs and relax to the lowest energy levels within a short time scale (∼1–100 ps). In practice, even or odd carrier numbers in the QD are possible and have been observed. The detailed occupation depends on the excitation pump power and on the specific environment of the QD (e.g., donors, electric fields). And specific photons from the cascade process of sequential optical transitions of multi-exciton states, such as the XX and $1X$, can be spectrally filtered out and can be used to generate single photons. Due to the nonresonant excitation process the number of captured carriers in the QD is given by a Poisson distribution. To achieve a quantum efficiency close to unity for a certain transition, the pump power has to be adjusted well above the average occupation number of the corresponding transition. This has serious implications for the time jitter of the emission process. It is determined by the carrier capture times, the relaxation times within the dot, and the spontaneous emission time of the corresponding transition. A typical jitter is in the range between several 100 ps up to a few nanoseconds. Another drawback of the nonresonant excitation process is that charge carriers can be captured by adjacent traps or defect centers in the vicinity of the dot. This might lead to fluctuations in the emission wavelength between different pulses and is known as spectral diffusion, a major line broadening effect for QD transitions. In addition, pure dephasing occurs due to elastic scattering with other carriers. This will further reduce the indistinguishability of the photons.

In contrast, the quasi-resonant excitation into a higher shell of the p-shell has some important advantages against the non-resonant pumping scheme discussed above. While the above-barrier excitation might be approximately considered as an incoherent excitation process, the p-shell pumping can be arranged as a coherent process. This opens the possibility of a controlled occupation of one electron–hole pair in the p-shell by applying a π-pulse. After relaxation into the s-shell, each generated electron–hole pair delivers a single photon. Thus, high quantum efficiency (close to one) can be possible. Another important aspect is a nearly complete suppression of background light for quasi-resonant pumping. This leads to an almost complete suppression of multiple ($n \leqslant 2$) emission events and therefore nearly perfect triggered single photon emission is achieved [$g^{(2)}(0) \sim 0$] [58]. In addition, pure dephasing processes should be drastically reduced since the charge carriers are exclusively generated within the desired QD.

As another case shown in Fig. 6, the ultimate pumping process would be a direct excitation into the s-shell of the QD. Using a π-pulse, exactly one of the two optically bright exciton states could be excited. This scheme possesses the same advantages as the quasi-resonant excitation scheme, but in addition, no additional relaxation process would be necessary before the photon emission process. That would reduce the time jitter to solely the radiative lifetime. Furthermore, the polarization of the photon used in the excitation process is carried to the emitted photon if spin relaxation could be neglected. Notably, Mueller and coworkers [59] have recently demon-

strated resonance fluorescence from a coherently driven semiconductor QD in a cavity. The QD was embedded in a planar optical microcavity and excited in a wave-guide mode so as to discriminate its emission from residual laser scattering. This promises both improved photon indistinguishability and high efficiency. Remarkably, by applying resonant s-shell optical excitation with picosecond laser pulses, Pan and coworkers from USTC have recently generated pulsed single photons on demand from a single, microcavity-embedded QD under s-shell excitation with 3 ps laser pulses, significantly eliminating the effect of decoherence, and have further used two single photons to implement a high-fidelity quantum controlled-NOT gate. The π pulse-excited resonance-fluorescence photons have less than 0.3% background contribution and a vanishing two-photon emission probability. Non-postselective Hong–Ou–Mandel interference between two successively emitted photons is observed with a visibility of 0.97(2), comparable to trapped atoms and ions. Besides, resonant electrical pumping could be achieved with double-heterojunction resonant-tunneling structures as proposed in Ref. [5].

Other excitation schemes like stimulated Raman scattering involving adiabatic passage (STRAP), or variants of them, have been demonstrated in atomic systems [35, 60] for the controlled generation of single photons. These schemes allow an active control of both the excitation and decay processes in a *coherent* way. Therefore, they transcend the temporal separation of the excitation and decay process and promise a high degree of indistinguishability of the single photons. However, these techniques rely on two tunable lasers or one laser and a high finesse cavity exactly tuned to the desired transition which requires a rather elaborate labor work.

4 Localization of single quantum dots coupled to cavities

The presence of a cavity strongly affects the available photon density of states (PDOS) of the environment. When a quantum emitter is placed inside a cavity, many properties of its light emission can be strongly modified [25, 32]. Spontaneous emission rate and radiative decay can be engineered and enhanced, radiative pattern and divergence angles can be modified to improve collection efficiency and optical matching with optical fibers, spectral emission can be narrowed or filtered and the emission polarization can be controlled. Micro and nanocavities embedding quantum emitters are the subject of intensive studies for the realization of ultralow threshold nanolasers [5, 23, 25], or cavity-QED [1, 3, 35]. Cavity-QED systems allow us fundamental studies of coherent interactions of confined electromagnetic fields (cavity photons) and microscopic dipoles (single quantum emitters) [1, 3, 35]. The task of aligning a single quantum emitter to a cavity is very challenging since its single exciton transition must be coupled to a resonant mode of a high quality factor (Q-factor) microcavity. When this is achieved, the efficiency and emission properties of a single QD are significantly improved. The coupling between the quantum emitter and the cavity can be either strong or weak depending on the coupling parameter,

$$g = \frac{\mu_d}{\hbar}\sqrt{\frac{\hbar\omega}{2\varepsilon_0 V}} \tag{44}$$

where V is the cavity mode volume, ε_0 is the vacuum dielectric constant, and μ_d is the dipole moment of the transition. Strong coupling occurs when the emitter–photon interaction becomes larger than the combined atomic dipole decay rate and the cavity field decay rate. The regime of strong coupling between a single exciton confined in a QD has been achieved in microcavity systems based on microdiscs [2] in photonic crystal nanocavities [3] and in pillar microcavities [4, 33]. In all these structures, quantum electrodynamic (QED) effects of zero-dimensional electron systems interacting with optical modes, like the Purcell effect or Rabi splitting, have been observed [1–5, 25, 59]. As a comparison, weak coupling enhances the spontaneous emission, whose rate is given by the Purcell factor

$$F_p = \frac{3}{4\pi^2}\frac{Q}{V}\left(\frac{\lambda}{n}\right)^3 \tag{45}$$

When a QD is embedded into the microcavity, its eigenfrequency ω_0 is resonant with the high-Q cavity mode ω_c and $g^2 > (\gamma-\kappa)^2/16$, with κ and γ, the cavity field decay rate in free space of the environment and the QD decay rate inside the cavity mode, respectively. This leads to a new strongly coupled quantum system which evolves with a coupling strength defined by the vacuum Rabi splitting [1–5, 25]. In both strong and weak coupling, the target is to reduce the modal volume of microcavity or photonic crystal nanocavities. When F_p is greater than 1, the quantum emitter radiates faster in the cavity than in free space and the emission is enhanced as long as the system remains in the weak coupling regime. The coupling is maximized when the emitter is placed in the maximum of the electric field intensity; however, this is hard to be fulfilled for point-like emitters, since it requires a very high accuracy in QDs positioning inside an ultrasmall volume of microcavity or photonic crystal nanocavity [3].

To align the quantum emitter to a microcavity or to

fabricate arrays of single photon source devices in specific locations, both epitaxial self-assembled QD and colloidal NCs as point-like emitters, one of the most challenging tasks is the precise control over the QD position. The typical way to realize a single photon source based on self-organized QDs is to inspect the sample purposely fabricated with low density of QDs ($\ll 10^9$ cm^{-2}). After having localized an isolated area with a single nanostructure inside, we build a device using very high resolution fabrication techniques [61–63]. The nucleation sites, and therefore the surface density of epitaxial QDs, are usually controlled by carefully tuning the Stranski-Krastanov growth parameters. Colloidal NCs are typically diluted to nanomolar concentrations and dropcasted on glass cover slides, and obtain, after evaporation of solvents, isolated nanocrystals with an average distance among them in the order of microns. Though well-suited for the characterization through confocal microscopy of photon antibunching behavior in single nanostructures [21, 54], these approaches are not appropriate for the controlled arrays of single photon source to be embedded in QKD commercial systems. Although the QDs are formed on random positions on the wafer, nanolithographic technique allows to control the QD position by pre-patterning the growth surface of the wafer. This active positioning is a considerable progress with respect to the applications of single QDs for single-photon sources. In the past few years, fabrication of controlled pre-patterned recesses in the substrate and regrowth has been successfully exploited [64] with a hope to embed single QDs into micropillar cavities [4, 33, 65] and 2D photonic crystal membranes [66] to localize epitaxial QDs. On the other hand, doping of vertical microcavities with an ensemble of NCs has been demonstrated by different techniques, by embedding the NCs in two distributed Bragg reflectors (DBRs) [67] and by focused ion beam (FIB) post–milling to obtain micropillars [29] or by imprint lithography [68]. Coupling of a single colloidal QD with photonic cavities has been achieved by exploiting whispering gallery modes generated on the surface of glass and polymer microspheres [69]. Artemyev *et al.* [69] reported on the coupling of a single CdSe/ZnS NCs chemically bound to the surface of a single glass microsphere, and report the Purcell factor $F_p \sim 10$. The same group reported on a strongly coupled cavity-QED system consisting of an anisotropically-shaped CdSe NC coupled to a single photon mode of a polymer microsphere, showing a vacuum Rabi splitting between 30 and 45 μeV in a microsphere cavity, slightly deformed to remove mode degeneracy [61].

To the best of our knowledge, few papers in the literature has reported on efficiently emitting triggered single photons with single colloidal NCs embedded in microcavities at room temperature so far, and the lack of single photon emission up to room temperature prevents their practical use. Recently, a new approach has made possible the pinpointing of single colloidal QDs by direct electron beam lithography. The controlled localization of ordered arrays of single colloidal NCs was demonstrated in Refs. [70, 71] by dispersing a specific concentration of NCs inside a negative high-resolution electron-beam resist after precipitation and re-dilution in methyl-isobutyl-ketone (MIBK) solvent. Ensembles of NCs embedded in electronic resists can be easily patterned by means of traditional lithographic processes since the presence of semiconductor clusters in the matrix does not significantly affect the sensitivity of the polymeric host and, at the same time, the emission properties of the NCs are not influenced by the interaction with the electron beam [71, 72]. Through a careful control of molar density of the NCs dispersed in the resist and pillar volume, i.e., through blending layer thickness and pillar diameter, it is possible to obtain a very high probability of having localized single colloidal NCs, whose photon antibunching behavior was confirmed through a confocal microscope and Hanbury–Brown and Twiss setup [4, 21, 54]. It is worth noting that asymmetric NCs, such as nanorods and QD-in-rods, are particularly suitable for the achievement of strong coupling regime since they exhibit a strong dipole moment and increased dipole oscillator strength [12, 73]. Besides electrostatic trapping is very attractive for NCs of asymmetric QD-in-rods with a high dipole moment.

5 Single-photon sources

Both epitaxial self-assembled QD and colloidal NCs have been used as active media of single photon sources.

In this section we give a discussion of recent novel development on semiconductor QD-based single photon sources. The two approaches report progress on one or more of the following properties, e.g., extension of the demonstrated wavelength range, high single-photon emission rates, polarization control, electrical pumping, single photon emission in the strong coupling regime, photon indistinguishability, high temperature operation, and on-chip QD-based single photon sources.

5.1 Wavelength engineering and high single-photon emission rates

For practical applications the emission wavelength of the single photon source should be one which minimizes op-

tical losses in the transmission and maximizes the photon detection efficiency. Currently, Si-Avalanche photodiodes are the most efficient single photon detectors. They possess the highest quantum efficiency (∼70%–75%) in the wavelength range 630–750 nm. The emission wavelength of the source should be within the absorption minimum of the transmitted medium. For free space applications this is fulfilled in the visible spectral region, for a plastic optical fiber within an absorption minima of the fiber (560 nm, 650 nm), and for a glass fiber at 1.3 μm (dispersion minimum) and around 1.55 μm (absorption minimum). Since the first demonstration of single-photon emission on the basis of a single QD [28], extensive studies on single-photon sources have been performed on a wide variety of semiconductor compound QDs such as $In_xGa_{1-x}As/GaAs$ (∼870–970 nm) [2–5, 74], $In_xGa_{1-x}As/Al_yGa_{1-y}As$ (∼800–815 nm) [75, 76], $GaAs/Al_xGa_{1-x}As$ (∼735–790 nm) [77], $In_{0.75}Al_{0.25}As/In_{0.7}Ga_{0.3}As$ (∼770 nm) [78], CdSe/ZnS colloidal NCs [39], InP/GaInP (∼669.0 nm in the red spectral range) [79, 80]. In addition, single photon emission at the telecom wavelength ∼1.3 μm has also been realized [81, 82].

In 2011, Bommer *et al.* [79] have performed systematic excitation power and temperature-dependent measurements on the emission lines of single self-assembled $InP/(Al_{0.20}Ga_{0.80})_{0.51}In_{0.49}P$ QDs embedded in micropillars. To enhance the photon collection efficiency, the QD layer is additionally sandwiched between distributed Bragg reflectors (DBRs) forming a planar microcavity. Besides, the exciton and biexciton intensity, linewidth, and spectral position was investigated in a temperature range from 4 K up to 130 K. InP QD sample structures with aluminum containing barrier layers have been chosen to improve the charge carrier confinement and thus the high temperature operation of non-classical photon emission. By using self-assembled QDs embedded in a planar microcavity realized by monolithically grown AlGaAs DBRs, single-photon emission from the QDs is presented up to a temperature of 100 K, confirmed by photon-statistics measurements [79]. This is a promising result since in micropillar cavities the signal rate should be even higher due to a better mode confinement. The operation wavelength is within a transmission minimum of the plastic optical fiber and is well suited for free space applications. Note that InP QDs with their emission wavelength in the red spectrum are of especial interest as single photon sources because the Si-photodetectors that are used for photon detection have the highest quantum efficiency in the red spectral window. Furthermore, Ugur *et al.* [80] have very recently achieved diluted QDs with densities as low as 1 dot/μm^2 using ultra-low-rate epitaxy to allow the observation of single QD emission without apertures or post-growth processing. As shown in Fig. 7(a), both excitionic and biexcitonic emissions are observed from single QDs created in this way, appearing as doublets with a fine-structure splitting of 320 μeV. The autocorrelation value of $g^{(2)}(0) = 0.2088 \pm 0.0538$ is obtained by using the Hanbury Brown–Twiss correlation measurements under cw excitation, showing antibunching behavior [in Fig. 7(b)]. The polarization of the split states has also been investigated. Besides, they observed single photon emission rates of 1.55 MHz. At this step, it should be pointed out that several sources are used as single photon sources, i.e., atoms, ions, nitrogen vacancy-centers which can have single photon emission but with rates below MHz [12–15]. Only for epitaxial QDs, high speed single photon emission with a rate as high as several MHz has been achieved [40, 79, 80, 83].

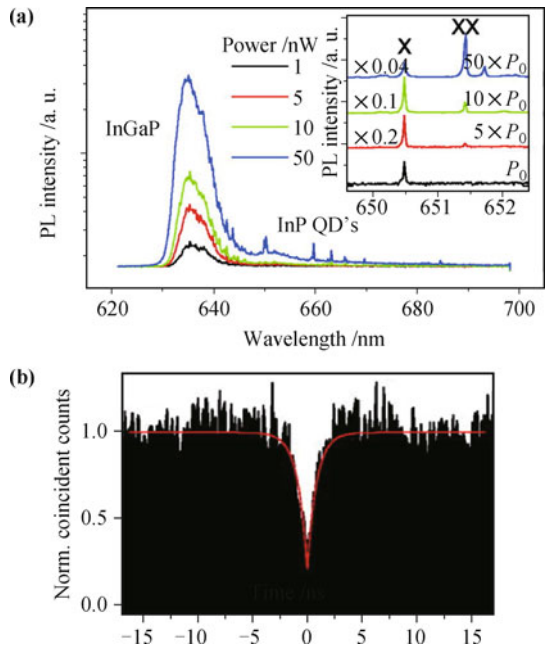

Fig. 7 **(a)** PL spectra for a low-density QD ensemble. The emission at 630 nm originates from the InGaP and the emission at 650–670 nm from InP QDs. Inset graph is a magnified view of the spectrum from one of the single QDs; both excitonic (X) and biexcitons (XX). **(b)** Second order correlation function of X from InP QD. Reproduced from Ref. [80], Copyright © 2012 American Institute of Physics.

For many applications in quantum information technology the single-photon source should provide a single polarization of the emitted photons together with high single-photon emission rates. The origin of the usually observed strong polarization degree in the emission is twofold. First, photons are preferentially emitted into the polarized mode due to the Purcell effect, which prepares the photon into a given quantum state. Second,

the polarized emission is more efficiently collected by a collection lens due to the directionality of the mode profile. Both properties can be realized by embedding a QD in an appropriate cavity structure. Polarization degrees higher than 90% have been found in the emitted light in one linear polarization state [33, 80]. The polarization of the emission of a QD, e.g., from an excitonic transition, depends on the spin state of the exciton. For QDs outside a cavity there is no preferred polarization since both spin states are equally likely. For QDs inside the cavity the mode structure in which the QDs can emit is modified. A more sophisticated device would also allow for an active selection of the polarization states on the chip, e.g., with an applied external field. In 2007, Strauf and co-workers have realized such a single photon source where both high single-photon rates and control over the polarization state have been achieved [83]. The QDs were embedded into the center of a one-wavelength thick cavity which is sandwiched between two distributed Bragg reflectors. The two gates allow for controlling a QD loading process and a local current heating within the cavity. Trenches are fabricated to define oxide apertures and therefore optical mode-confinement. The design provides Q-factors up to 50 000 together with the possibility of controlling the mode degeneracy. Another important feature of the device is the record high single-photon emission rate. Under pulsed optical excitation, a single photon rate of 4 MHz has been achieved. In there, the excitation conditions have been chosen to a working point where $g^{(2)}(0) = 0.4$, that is, a point when the single photon source still performs 2.5 times better than an attenuated Poissonian source of the same average intensity. If corrected with the 13% detection efficiency of the setup the device emits into the first lens with a rate of 31 MHz. This ultrahigh rate is a combination of several effects. However, Stark-shift tuning will also be possible with their device design which should allow high modulation frequencies. Besides the already discussed effects of the Purcell enhancement and the large geometrical extraction efficiency of the cavity mode, two other reasons are responsible. To avoid signal losses by exciton relaxation to the dark states, the trion transition has been used as the optically active transition. This procedure increased the signal rate by a factor of three. Furthermore, a positive bias voltage created a fivefold intensity enhancement, most probably due to a field-enhanced carrier capture process.

In summary, ultrahigh single photon rates for QD-based single photon sources are already available at different wavelengths and in carefully designed semiconductor devices.

5.2 Electrical pumping of single photon sources

Electrically driven single-photon sources have also been demonstrated at different wavelengths and in different QD material systems. The first attempt on electrical pumping has been performed on a semiconductor heterostructure sample utilizing the Coulomb blockade effect in quantum wells at ultralow temperatures (some tens of millikelvin) [84]. The photon collection efficiency from the sample was weak, preventing the study of the photon correlation function. Shields *et al.* designed an efficient scheme based on a cavity structure at helium temperatures (5–10 K) [85]. Figure 8 shows a schematic of the single photon light-emitting diode (LED). The QDs are embedded in a 3λ-cavity which is sandwiched between a high-reflectivity bottom DBR and the semiconductor-air interface in the aperture. This low-Q cavity enhances the collection efficiency (tenfold) due to a modified emission pattern. A photon collection efficiency into a NA=0.5 lens of 4.7%±0.5% has been achieved. Single-photon emission has been demonstrated from the measured correlation functions for the exciton and the biexciton emission lines. The finite peak at delay time $\tau = 0$ is most probably caused by the background emission from the layers other than the QD. Electrical pumping scheme also opens the possibility to tailoring the time jitter, i.e., the uncertainty in the time of single photon emission events. By applying a negative bias to the diode between the electrical injection pulses, using a resonant cavity LED, Bennett *et al.* [86] reduced the jitter in the photon-emission time to less than 100 ps, i.e., one-fifth of the radiative lifetime. This allowed the repetition rate of the single-photon source to be increased to 1.07 GHz while retaining good single-photon emission characteristics. This idea may lead to a new method by which pairs of indistinguishable photons can be generated for photonic quantum logic experiments.

In 2007, Ward *et al.* [87] demonstrated an electrically driven telecommunication wavelength (∼1.29 μm) single-photon source at low temperature (∼12 K), in which negative-going 0.5 V pulses (∼10 ns) have been applied to the device shortly after each positive-going excitation pulse to reduce the time jitter. The large InAs/GaAs QDs possess a higher electronic confinement potential, which allows the emission to be Stark shifted out of the passband of the used spectral filter (FWHM∼0.5 nm) before all carriers are removed from the QD. In addition, they proposed that the time-varying Stark shift also allows to eliminate multiphoton emission processes due to reexcitation during the relatively long (220 ps) electrical pump pulses. Recently, Heindel *et al.* [88] have presented triggered single photon emission from low mode volume

electrically driven QD-micropillar cavities at repetition rates of up to 220 MHz. Due to an optimized layout of the doped planar microcavity and an advanced lateral current injection scheme, highly efficient single photon sources are realized. While $g^{(2)}(0)$ values as low as 0.13±0.05 and a Purcell factor of 4 are observed for a 2.0 μm diameter micropillar, single photon emission at a rate of (35±7) MHz and an overall efficiency of (34±7)% are demonstrated for a 3.0 μm device.

Another interesting approach is to use an aperture in an oxide layer to restrict carrier injection into a single QD [25, 89, 90]. This technique has been already successfully used in the VCSEL technology for current and mode confinement [24, 25]. A thin AlAs layer is grown some 10 nm above the QD layer within the intrinsic region of the p–i–n layer of the device. After a mesa structure has been fabricated a wet oxidation process is performed to convert the outer edge of the AlAs layer to insulating AlO_x. Apertures down to 100 nm diameter can be produced. The advantages of such a design are lower injection currents, lower background emission since ideally only one QD is excited, a good lateral mode confinement together with mechanical stability. The observation of Purcell enhancement in the decay rate of a single QD by electroluminescence of such a device has been reported in an electrically driven oxide confined LED structure [91]. This allowed single photon electroluminescence up to repetition rates of 0.5 GHz. Besides, it is very important for quantum communication applications to develop electrically driven sources at elevated temperatures. This may be achieved by using wide-bandgap semiconductors and other alloys providing high quantum confinement. In 2008, an electrically driven single-photon emitter in the visible spectrum range, working up to 80 K, has been realized by a p–i–n diode structure with InP QDs as active layers in the red spectral range at speeds of up to 200 MHZ [92]. The InP QDs were embedded between two 30nm thick $Al_{0.2}Ga_{0.8}InP$ layers that were sandwiched between two 100 nm thick $Al_{55}Ga_{45}InP$ layers. This design ensured both good carrier confinement and high internal quantum efficiency. In their experiment, clear photon antibunching [$g^{(2)}(0) = 0.43$] is observed, and after deconvolution with the experimental response function and subtracting the background value of 0.03 for $g^{(2)}(0)$, a value of $g^{(2)}(0) = 0.25$ was determined. This result demonstrates that even at 80 K, these QDs are suitable to provide electrically driven single-photon emission. At that point it is not clear if even higher temperatures can be reached with this dot system due to a possible spectral overlap between exciton and biexciton lines which would degrade the purity of single photon emission.

On the other hand, injection of carriers in colloidal NCs is not as straightforward as for epitaxial QDs, where these nanostructures can be directly embedded in p–n junctions. Direct injection of charge carriers in colloidal NCs is typically limited due to the presence of an insulating organic capping layer on the NCs. Although most experimental results on photon antibunching and single photon sources are based on optical pumping of QDs, colloidal NCs have demonstrated their potential in many applications because of their aforementioned peculiar properties. The approach for electrical pumping of colloidal NCs embedded in single photon source devices and light emitting devices are currently being pursued. This approach has been already exploited for the demonstration of white light LEDs based on colloidal NCs on nitride–based quantum wells LEDs [89].

5.3 Single-photon emission in the strong coupling regime

In 2007, Ester *et al.* reported on deterministic single photon emission after coherent optical state preparation in the *p*-shell of a single InGaAs/GaAs QD [93]. Under the condition of π-pulse excitation into the *p*-shell they demonstrated nearly perfect single photon emission [$g^{(2)}(0) = 0.02$]. However, a high degree of indistinguishability and quantum efficiency cannot be realized in case of an excitation scheme via an excited state in the QD simultaneously. Therefore, a truly resonant pumping scheme would be advantageous. Recently, Mueller *et al.* have reported the first measurement of resonance fluorescence in a single self-assembled QD [59]. Both continuous wave and pulsed optical excitation (8 ps long pulses) have been realized by the group and a full Rabi cycle has been achieved in the single QD resonance fluorescence under the latter. As shown in Fig. 8, the QD is embedded in a planar optical microcavity and excited in a waveguide mode so as to discriminate its emission from residual laser scattering [59]. Continuous wave second-order autocorrelation measurements revealed a pronounced antibunching dip and further confirmed nonclassical light emission, demonstrating the successful generation of

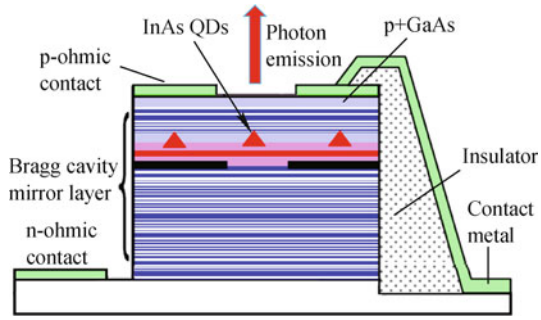

Fig. 8 Schematic structure of the single-photon LED.

single photons.

Single-photon emission in the strong-coupling regime has been observed from a QD-micropillar cavity [4, 29, 33, 65, 79, 88, 94] and from a QD-photonic crystal cavity [3, 62]. The strong-coupling regime is of great interest for many quantum information schemes.

In the QD-micropillar cavity system, a quasiresonant excitation via an excited state has been performed which mostly prevented background emitters from being excited. Press *et al.* [94] observed photon antibunching in the photons emitted from a strongly coupled single quantum dot and pillar microcavity in resonance. Quasiresonant pumping of the selected QD via an excited state enabled these observations by eliminating the background emitters that are usually coupled to the cavity. A coupling constant of $g = 35$ μeV and a mode linewidth of $\gamma_c = 85$ μeV have been reported [94], which satisfies the strong coupling condition. They demonstrated an on-demand single-photon source operating in the strong coupling regime with a Purcell factor of 61±7 and quantum efficiency of 97%. Furthermore, Schneider *et al.* [65] have successfully demonstrated the deterministic integration of single site-controlled QDs into micropillar cavities. Spatial resonance between single positioned QDs and GaAs/AlAs micropillar cavities was achieved using cross markers for precise QD-cavity alignment. Single photon emission from a spatially and spectrally site-controlled coupled QD-resonator system is confirmed by photon autocorrelation measurements yielding a $g^{(2)}(0)$ value of 0.12.

In the case of the QD photonic-crystal cavity, nonresonant excitation into the barrier has been realized. In 2007, Hennessy *et al.* realized a positioning of an individual QD relative to the photonic crystal cavity with a 30 nm accuracy [17, 62]. Therefore, the QD was located typically at ∼90% of the electric-field maximum. When off-resonance, photon emission from the cavity mode and QD excitons is anticorrelated at the level of single quanta, proving that the mode is driven solely by the QD despite an energy mismatch between cavity and excitons. When tuned to resonance, a coupling constant of $g = 76$ μeV and a mode linewidth of $\gamma_c = 100$ μeV have been achieved, and the exciton and cavity enter the strong-coupling regime of cavity QED. The QD exciton lifetime reduces by a factor of 145 [62]. The generated photon stream becomes antibunched, proving that the strongly coupled exciton/photon system is in the quantum regime However, the autocorrelation only exhibits a value of $g^{(2)}(0) = 0.54$, indicating a lower purity of the single-photon emission than in the micropillar case discussed above.

In the case of a single photon source it has been anticipated that extremely high efficiency and photon indistinguishability could be achieved [10]. In the strong coupling regime the decay rates of the coupled QD cavity system are typically short. In the aforementioned studies values in the 10–20 ps range have been reported. To avoid multiple capture and emission processes from the emitter after a single laser excitation pulse, resonant or quasiresonant excitation schemes are essential to achieving the high-purity single photon emission $g^{(2)}(0) \sim 0$. Otherwise, in the case of above barrier pumping process, long lived excitons may be captured by the QD after the emission of a first single photon pulse, which leads to multiple photon emission processes. From the discussion above it becomes clear that both resonant-pumping and a positioning of a single quantum dot relative to the microcavity would be highly advantageous.

5.4 High temperature operation

From the viewpoint of practical applications, e.g., in quantum cryptography, it would be important to be able to operate the single-photon sources at elevated temperatures or even at room temperature without any cooling. For high-temperature operation several requirements have to be met. First, large electronic band offsets and strong quantum confinement effects for both electrons and holes are necessary in order to prevent the carrier thermalization and thermal emission of carriers into the wetting layer and/or barriers. Second, a large biexciton binding energy is important to prevent spectral overlapping of exciton and biexciton recombination lines at elevated temperatures [95–97]. Wide-bandgap semiconductors like II–VI- and group-III nitride semiconductors offer large biexciton binding energies [95–98], and therefore the material system has turned out to be a key factor for the device operation at elevated temperatures. The well-established InGaAs/GaAs system allowed for essential progress in single photon sources like efficient control of the light outcoupling. However, the weak carrier confinement limits the operation of these photonic devices to low temperatures. The operation temperature has been raised meanwhile up to 80 K in electrically driven InP/(In,Al)GaP-QDs and up to 200 K in Ga(In)N/GaN [95], and 220 K in CdZnSe/ZnSe [97] in optically excited structures. The (Cd,Zn)Se system seems to be most promising for that purpose, because both photoluminescence and electroluminescence from a single QD were observed up to 300 K [97, 98]. However, it is until very recently that single photon emission at room temperature has been demonstrated and room temperature operation (300 K) has been reported on the basis of the CdSe/ZnSSe material systems [99].

In 2006, Kako *et al.* [95] reported triggered single photon emission from GaN/AlN QDs at temperatures up to 200 K. In their experimental PL spectra under pulsed excitation, the selected exciton line at 3.5 K exhibits a relatively broad linewidth, which is most probably due to spectral diffusion. The biexciton at slightly higher energy is clearly separated from the exciton line. The second-order coherence function of photon-correlation histograms using the Hanbury Brown–Twiss set-up under continuous-wave excitation is depicted in Fig. 9. A value of $g^{(2)}(0)$ of 0.42 has been obtained at 3.5 K. A clear antibunching effect is observable at temperatures up to 200 K, though at 200 K the exciton and biexciton lines are no longer clearly separated due to phonon broadening. The two-photon probability increases slightly to 0.53 most probably due to a partial overlap with the biexciton line. In addition, a broadband background from the AlN matrix contributes to the detected signal. In 2007, Arians and co-workers reported the luminescence from a single CdSe QD at room temperature [96]. In this case the self-assembled QDs were embedded in ZnSSe/MgS barrier layers, which provide a higher electronic confinement than bare ZnSSe layers. As is very promising, the intensity dropped by less than a factor of 3 between 4 K and room temperature. The room temperature linewidth of the single QD emission was 25 meV, which is attributed by the authors to the interaction of excitons with optical phonons. Very recently, Fedorych *et al.* [99] have reported room temperature single photon emission from self-assembled epitaxially grown CdSe/ZnSSe/MgS QDs under continuous wave optical excitation. CdSe/ZnSSe QDs are embedded into MgS barriers, providing dominant radiative recombination up to 300 K. Under continuous wave optical excitation, the autocorrelation function $g^{(2)}(t)$ exhibits a sharp dip at $(t = 0)$ with $g^{(2)}(0) = 0.16 \pm 0.15$ at $T = 300$ K, revealing excellent suppression of multiphoton emission even at room temperature.

5.5 On-chip QD-based single photon sources with photonic crystal nanocavities

On-chip QD-based single photon sources are one of the key components for integrated quantum photonic circuits. Micro- and nano-scale cavity resonators, such as micropillar cavities [4, 29, 33, 65, 79, 88, 94], microdiscs [2, 25], and photonic crystal nanocavities [3, 25, 62, 63, 100–105], represent viable resonator choices depending on the particular applications. The photonic crystal nanocavities are point defects embedded within periodic dielectric structures [3, 17, 63, 100, 101], where photons are completely localized in the vicinity of the defects [3, 102]. As a result, photonic crystal nanocavities have gained widespread interest due to their high Q factor ($> 1 \times 10^6$ even up to 2×10^7 in the optimized structure) with extremely small mode volumes comparable to a wavelength dimension [3, 100, 103]. The photonic crystal nanocavities can be easily tuned by bringing a nanostructure into the near field of the cavity [25, 63, 100, 104]. These features offer predominant conditions for reaching an extremely strong light-matter coupling regime with current state-of-the-art nanocavities. On the other hand, although glass spherical cavities and micropillar cavities localize very high quality factor modes, their use as single photon sources is hindered due to their relatively large mode volume and their poorly collimated photon emission [3, 103]. Strong localization is essential for strongly enhancing the interaction strength between the photons and the QDs [1–3, 25]. In this respect, photonic crystal nanocavity structures are promising candidates for the trapping of light in ultrasmall volumes with high Q-factor [3, 100–106].

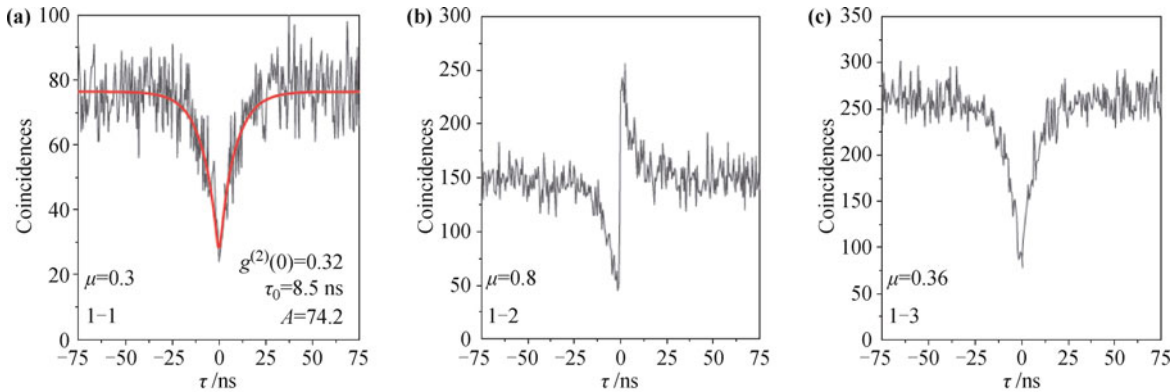

Fig. 9 Histograms under continuous-wave excitation as a function of the relative delay between photons detected by the "start" and "stop" at the time-interval counter. **(a)** Auto-correlation of peak 1. The solid red line and numbers show the fitting curve and fitting parameters, respectively. **(b, c)** Cross-correlation between peaks 1–2 and peaks 1–3, respectively. Each number corresponds to the peak as indicated in (a). Lines show the fitting curves as mentioned in the text. Reproduced from Ref. [95], Copyright © 2006 Nature Publishing Group.

Banaee *et al.* [106] have proposed and investigated the unidirectional coupling of a microcavity mode to a ridge waveguide in a slab photonic crystal structure. Their experimental result of the coupling efficiency for the signal coupled out of the structure is in good agreement with the result of three-dimensional finite-difference time-domain (FDTD) simulations. The coupling efficiency of the cavity mode to the output channel is ~60%. With the integrated coupler, more than 60% of the emitted field overlaps with the output waveguide mode. Stimulated by the enhanced Purcell factors of a photonic crystal waveguide and efficient unidirectional collection of the emitted photons, Hughes *et al.* have proposed a "single photon gun" based on a small section of a photonic crystal waveguide near the slow-light mode integrated with an output coupler [107]. Furthermore, as shown schematically in Fig. 10, a concept device of single photon source that exploits some of the advantages of integrated cavities, waveguides, and couplers were also proposed [107, 108]. Here, although the increased coupling between the cavity and the waveguide leads to the decrease of the Purcell factor compared to the bare cavity, the major advantage is that on-chip emission is possible with the integrated waveguide. The spatial distribution of the field at the maximum Purcell factor shows how the emitted field leaks predominantly into the output waveguide [108]. We highlight that the peak Purcell factor is certainly larger than that required to enter the strong coupling regime for a typical QD exciton. Another interesting application using a strongly coupled single-QD-cavity system is for electro-optic modulation in integrated quantum photonic circuits [25, 109]. This has already been demonstrated by using just a single photonic crystal cavity with a strongly coupled QD, which was probed with use of reflectivity measurement [110]. In this case, the cavity is butt-coupled to two photonic crystal waveguides that serve as the input and output ports. In this case, however, the cavity is now deliberately *over-coupled* to the

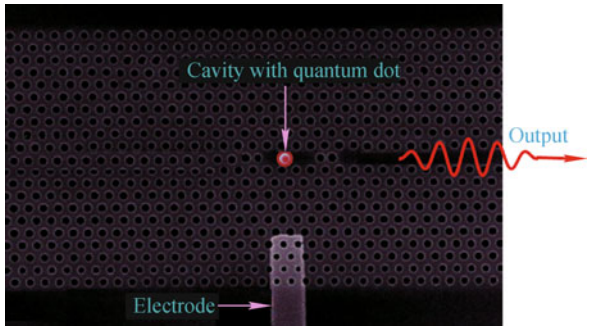

Fig. 10 Schematic diagram of waveguide-cavity single photon source, which is composed of one photonic crystal cavity and one waveguide, one QD (denoted by red-purple dot) is placed within the cavity.

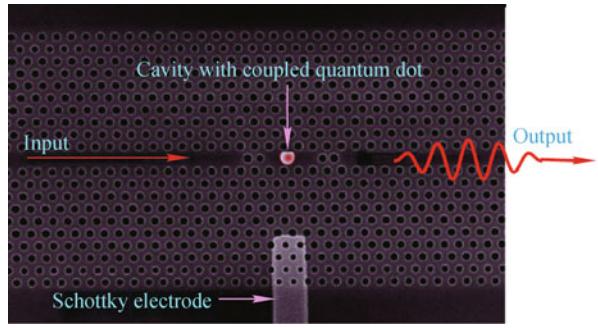

Fig. 11 Integrated photonic concept device for on-chip optical signal processing. The QD frequency can be changed using a bias electric field applied via a Schottky electrode.

PC waveguide; and the PC waveguide is then coupled to an output wire waveguide.

Nano-photonic devices and integrated quantum photonic circuits based on quantum optical effects at the single-QD-emitter and single-photon level represent a fundamental technological limit for the on-chip processing of classical and quantum information [3, 25, 109]. One of the solid-state quantum emitters that is most suitable for integration is the InAs QD in GaAs because of its excellent optical properties and the well-developed GaAs semiconductor fabrication techniques [1–3, 25, 66, 106]. With InAs QDs, quantum information can be encoded in the spin of electrons or holes that can be completely manipulated using fast optical pulses [25, 111]. The advantage of using photonic crystal nanocavities is that they have extremely small optical mode volumes in a tiny space of optical-wavelength dimension [3, 103, 104] and are well suited for the integration with optical waveguides and on-chip integrated quantum photonic circuits [8, 25]. Recently, demonstrated techniques for efficient electrical injection into photonic crystal cavities [112] could also be employed in single QD based single-photon sources.

Though the crucial step for the fabrication, i.e., the positioning of single QDs in the resonant path of the nanocavity modes, is very difficult to be achieved, for future improvements, it can be anticipated that the collection efficiency can be further increased if we increase the coupling between waveguide and cavity by resizing or reducing the air hole radius at the interface between cavity and waveguide. In general, photonic crystal nanocavities with waveguides that can provide a well collimated emission are more suited for the realization of single photon sources [3, 105, 107].

6 Conclusions and outlook

This review has discussed recent progress and encour-

aging technological approaches in understanding the physics of the single photon sources based on single QDs, which is a building block for the future quantum information. The on-demand single photon source is an extremely important source for quantum information science and technology. Important progress has been achieved in the understanding of the QD excitation process and its role on the coherence time of the photons, on the limitations of photon indistinguishability and collection efficiency, on cavity effects on single photon emission, and on the influence of the excitonic fine structure (dark states) on emission efficiency. Spectacular achievements include the extension of the wavelength range from the UV spectral region (350 nm) up to the near infrared (1.3 μm), polarization control and the demonstration of ultrahigh measured single-photon emission rates (∼4 MHz), room temperature operation with wide bandgap semiconductor QDs, electrical pumping with a cavity design for enhanced photon collection efficiency, electrical pumping up to 80 K with an improved heterostructure design, high-purity single photon emission [$g^{(2)}(0) \sim 0.02$], the generation of high degrees of photon indistinguishability (97%), coherent state preparation in the *p*- and *s*-shell of an individual QD, single-photon emission from positioned QDs in cavities, and single-photon emission in the strong coupling regime.

However, despite the remarkable progress done so far, many challenging issues remain to be overcome and some of the technological problems need to be solved. Manipulation, embedding and positioning into the microcavities and efficient electrical pumping of single QDs are technological subjects discussed in this review, which still need to find optimal solution to. Moreover, one important issue is that most of the aforementioned achievements have been individually realized, but not realized in combination. Meaningful combinations strongly depend on the specific application of the single-photon source. However, we have witnessed the pioneering experiments and impressive performances reported in the literature in the past few years, which makes triggered sources of single photons closer and closer to their practical application in quantum communication and quantum cryptography.

As the potential suitable solid-state material of choice, we believe that the prospects for using integrated photonic crystal chips with photonic crystal nanocavity and waveguide offer many advantages for controlling and manipulating the light-matter interactions of an embedded QD. The improving semiconductor nanofabrication techniques and new and practical design insights have provided sound grounds for the optimism in envisioning what will come next. Furthermore, although enormous challenges remain, which include the understanding and possible control of decoherence processes, the role of fabrication imperfections, as well as the ability to deterministically position single QDs, we could certainly envision that, within the next few years, the community will achieve commercial products of on-chip QD-based single photon sources that could be built into semiconductor integrated photonic chips with integrated waveguide-cavity structures.

Acknowledgements G. Shan would like to thank Prof. C. Cohen-Tannoudji (Nobel Laureate in 1997) for his fruitful discussion on quantum optics and particularly theory of quantum-dot-cavity during his visit at City University of Hong Kong in 2012. This work was partially sponsored by General Research Grant Project No. CityU 119212 from RGC, Hong Kong, and the research activity fund from CityU to support research work as a visiting scholar at Columbia University. W. Huang acknowledges the support from the National Basic Research Program of China (973 Program, Grant No. 2009CB930601). Z. Yin acknowledges the support by the National Basic Research Program of China (973 Program, Grant Nos. 2011CBA00300 and 2011CBA00302), and the National Natural Science Foundation of China (Grant Nos. 61033001 and 11105136).

References

1. J. M. Gérard and B. Gayral, InAs quantum dots: Artificial atoms for solid-state cavity-quantum electrodynamics, *Physica E*, 2001, 9(1): 131
2. M. Pelton, C. Santori, J. Vuckovic, B. Zhang, G. S. Solomon, J. Plant, and Y. Yamamoto, Efficient source of single photons: A single quantum dot in a micropost microcavity, *Phys. Rev. Lett.*, 2002, 89(23): 233602
3. T. Yoshie, A. Scherer, J. Hendrickson, G. Khitrova, H. M. Gibbs, G. Rupper, C. Ell, O. B. Shchekin, and D. G. Deppe, Vacuum Rabi splitting with a single quantum dot in a photonic crystal nanocavity, *Nature*, 2004, 432(7014): 200
4. E. Peter, P. Senellart, D. Martrou, A. Lemaître, J. Hours, J. M. Gérard, and J. Bloch, Exciton-photon strong-coupling regime for a single quantum dot embedded in a microcavity, *Phys. Rev. Lett.*, 2005, 95(6): 067401
5. M. Pelton and Y. Yamamoto, Ultralow threshold laser using a single quantum dot and a microsphere cavity, *Phys. Rev. A*, 1999, 59(3): 2418
6. E. Knill, R. Laflamme, and G. J. Milburn, A scheme for efficient quantum computation with linear optics, *Nature*, 2001, 409(6816): 46
7. N. Gisin, G. Ribordy, W. Tittel, and H. Zbinden, Quantum cryptography, *Rev. Mod. Phys.*, 2002, 74(1): 145
8. N. Gisin and R. Thew, Quantum communication, *Nat. Photonics*, 2007, 1(3): 165
9. B. Lounis and M. Orrit, Single-photon sources, *Rep. Prog. Phys.*, 2005, 68(5): 1129
10. A. Muller, T. Herzog, B. Huttner, W. Tittel, H. Zbinden, and N. Gisin, "Plug and play" systems for quantum cryp-

tography, *Appl. Phys. Lett.*, 1997, 70(7): 793

11. G. Brassard, N. Lutkenhaus, T. Mor, and B. C. Sanders, Limitations on practical quantum cryptography, *Phys. Rev. Lett.*, 2000, 85(6): 1330
12. A. Kuhn, M. Hennrich, and G. Rempe, Deterministic single-photon source for distributed quantum networking, *Phys. Rev. Lett.*, 2002, 89(6): 067901
13. M. Keller, B. Lange, K. Hayasaka, W. Lange, and H. Walther, Continuous generation of single photons with controlled waveform in an ion-trap cavity system, *Nature*, 2004, 431(7012): 1075
14. B. Lounis and W. E. Moerner, Single photon on demand from s single molecule at room temperature, *Nature*, 2000, 407(6803): 491
15. C. Kurtsiefer, S. Mayer, P. Zarda, and H. Weinfurter, Stable solid-state source of single photons, *Phys. Rev. Lett.*, 2000, 85(2): 290
16. Y. M. He, Y. He, Y. J. Wei, D. Wu, M. Atature, C. Schneider, S. Hofling, M. Kamp, C. Y. Lu, and J. W. Pan, On-demand semiconductor single-photon source with near-unity indistinguishability, *Nat. Nanotechnol.*, 2013, 8(3): 213
17. A. Badolato, K. Hennessy, M. Atature, J. Dreiser, E. Hu, P. M. Petroff, and A. Imamoglu, Deterministic coupling of single quantum dots to single nanocavity modes, *Science*, 2005, 308(5725): 1158
18. X. Brokmann, L. Coolen, M. Dahan, and J. P. Hermier, Measurement of the radiative and nonradiative decay rates of single CdSe nanocrystals through a controlled modification of their spontaneous emission, *Phys. Rev. Lett.*, 2004, 93(10): 107403
19. J. Hu, L. S. Li, W. Yang, L. Manna, L. W. Wang, and A. P. Alivisatos, Linearly polarized emission from colloidal semiconductor quantum rods, *Science*, 2001, 292(5524): 2060
20. L. Manna, D. J. Milliron, A. Meisel, E. C. Scher, and A. P. Alivisatos, Controlled growth of tetrapod-branched inorganic nanocrystals, *Nat. Mater.*, 2003, 2(6): 382
21. G. Shan, S. Bao, C. H. Shek, and W. Huang, Theoretical study of fluorescence resonant energy transfer dynamics in individual semiconductor nanocrystal–DNA–dye conjugates, *J. Lumin.*, 2012, 132(6): 1472
22. I. N. Stranski and L. Von Krastanow, Abhandlungen der Mathematisch-Naturwissenschaftlichen Klasse, *Akademie der Wissenschaften und der Literatur in Mainz*, 1939, 146: 797
23. G. C. Shan and S. Bao, Theoretical study of a quantum dot microcavity laser, *Proc. SPIE*, 2007, 6279(1): 627925
24. A. Salhi, G. Rain, L. Fortunato, V. Tasco, G. Visimberga, L. Martiradonna, M. T. Todaro, M. De Giorgi, R. Cingolani, A. Trampert, M. De Vittorio, and A. Passaseo, Enhanced performances of quantum dot lasers operating at 1.3 μm, *IEEE J. Sel. Top. Quant.*, 2008, 14(4): 1188
25. G. C. Shan, M. J. Hu, C. H. Shek, and W. Huang, Vertical-external-cavity surface-emitting lasers and quantum dot lasers, *Front. Optoelectron.*, 2012, 5(2): 157
26. T. Akiyama, M. Sugawara, and Y. Arakawa, Quantum-dot semiconductor optical amplifiers, *Proc. IEEE*, 2007, 95(9): 1757
27. S. Kako, C. Santori, K. Hoshino, S. Gotzinger, Y. Yamamoto, and Y. Arakawa, A gallium nitride single-photon source operating at 200 K, *Nat. Mater.*, 2006, 5(11): 887
28. P. Michler, A. Imamoglu, M. D. Mason, P. J. Carson, G. F. Strouse, and S. K. Buratto, Quantum correlation among photons from a single quantum dot at room temperature, *Nature*, 2000, 406(6799): 968
29. M. Kahl, T. Thomay, V. Kohnle, K. Beha, J. Merlein, M. Hagner, A. Halm, J. Ziegler, T. Nann, Y. Fedutik, U. Woggon, M. Artemyev, F. Perez-Willard, A. Leitenstorfer, and R. Bratschitsch, Colloidal quantum dots in all-dielectric high-Q pillar microcavities, *Nano Lett.*, 2007, 7(9): 2897
30. T. Takagahara, Theory of exciton dephasing in semiconductor quantum dots, *Phys. Rev. B*, 1999, 60(19): 2638
31. C. Förstner, C. Weber, J. Danckwerts, and A. Knorr, Phonon-assisted damping of Rabi oscillations insemiconductor quantum dots, *Phys. Rev. Lett.*, 2003, 91(12): 127401
32. E. M. Purcell, Spontaneous emission probabilities at radio frequencies, *Phys. Rev.*, 1946, 69(11): 681
33. E. Moreau, I. Robert, J. M. Gérard, I. Abram, L. Manin, and V. Thierry-Mieg, Single-mode solid-state single photon source based on isolated quantum dots in pillar microcavities, *Appl. Phys. Lett.*, 2001, 79(18): 2865
34. C. Santori, D. Fattal, and Y. Yamamoto, Single-Photon Devices and Applications, Weinheim: Wiley-VCH, 2010
35. M. O. Scully and M. S. Zubairy, Quantum Optics, Cambridge: Cambridge University Press, 1997
36. R. Loudon, The Quantum Theory of Light, 3rd Ed., Oxford: Oxford Science, 2000
37. M. Scholz, T. Aichele, and O. Benson, Single-Photon Generation from Single Quantum Dots, Semiconductor Nanostructures (in Series of NanoScience and Technology), 2008: 329–349
38. A. J. Berglund, A. C. Doherty, and H. Mabuchi, Photon statistics and dynamics of fluorescence resonance energy transfer, *Phys. Rev. Lett.*, 2002, 89(6): 068101
39. A. Qualtieri, G. Morello, P. Spinicelli, M. T. Todaro, T. Stomeo, L. Martiradonna, M. De Giornia, X. Quelinc, S. Builc, A. Bramati, J. P. Hermier, R. Cingolani, and M. De Vittorio, Nonclassical emission from single colloidal nanocrystals in a microcavity: A route towards room temperature single photon sources, *New J. Phys.*, 2009, 11(3): 033025
40. P. Michler, A. Kiraz, C. Becher, W. V. Schoenfeld, P. M. Petroff, L. Zhang, E. Hu, and A. Imamoglu, A quantum dot single-photon turnstile device, *Science*, 2000, 290(5500): 2282
41. D. V. Talapin, R. Koeppe, S. Gotzinger, A. Kornowski, J. M. Lupton, A. L. Rogach, O. Benson, J. Feldmann, and H. Weller, Highly emissive colloidal CdSe/CdS heterostructures of mixed dimensionality, *Nano Lett.*, 2003, 3(12): 1677

42. C. M. Liddell, and C. J. Summers, Monodispersed ZnS dimers, trimers, and tetramers for lower symmetry photonic crystal lattices, *Adv. Mater.*, 2003, 15(20): 1715
43. Y. He, H. T. Lu, L. M. Sai, W. Y. Lai, Q. L. Fan, L. H. Wang, and W. Huang, Synthesis of CdTe nanocrystals through program process of microwave irradiation, *J. Phys. Chem. B*, 2006, 110(27): 13352
44. C. H. Bennett and G. Brassard, Int. Conf. Computers, Systems and Signal Processing, Bangalore, 1984, 1: 175
45. F. Pisanello, L. Martiradonna, P. Spinicelli, A. Fiore, J. P. Hermier, L. Manna, R. Cingolani, E. Giacobino, A. Bramati, and M. De Vittorio, Polarized single photon emission for quantum cryptography based on colloidal nanocrystals, *IEEE Proc. 11th Int. Conf. Transparent Optical Networks*, 2009: 1–4
46. A. Convertino, L. Cerri, G. Leo, and S. Viticoli, Growth interruption to tune the emission of InAs quantum dots embedded in InGaAs matrix in the long wavelength region, *J. Cryst. Growth*, 2004, 261(4): 458
47. O. G. Schmidt, Lateral Alignment of Epitaxial Quantum Dots (Springer NanoScience and Technology), Berlin: Springer, 2007
48. B. Mahler, P. Spinicelli, S. Buil, X. Quelin, J. P. Hermier, and B. Dubertret, Towards non-blinking colloidal quantum dots, *Nat. Mater.*, 2008, 7(8): 659
49. V. I. Klimov, A. A. Mikhailovsky, D. W. McBranch, C. A. Leatherdale, and M. G. Bawendi, Quantization of multiparticle auger rates in semiconductor quantum dots, *Science*, 2000, 287(5455): 1011
50. M. Nirmal, B. O. Dabbousi, M. G. Bawendi, J. J. Macklin, J. K. Trautman, T. D. Harris, and L. E. Brus, Fluorescence intermittency in single cadmium selenide nanocrystals, *Nature*, 1996, 383(6603): 802
51. X. Wang, X. Ren, K. Kahen, M. A. Hahn, M. Rajeswaran, S. MaccagnanoZacher, J. Silcox, G. E. Cragg, A. L. Efros, and T. D. Krauss, Non-blinking semiconductor nanocrystals, *Nature*, 2009, 459(7247): 686
52. S. A. Empedocles, D. J. Norris, and M. G. Bawendi, Photoluminescence spectroscopy of single CdSe nanocrystallite quantum dots, *Phys. Rev. Lett.*, 1996, 77(18): 3873
53. H. P. Lu and X. S. Xie, Single-molecule spectral fluctuations at room temperature, *Nature*, 1997, 385(6612): 143
54. L. Coolen, X. Brokmann, P. Spinicelli, and J. P. Hermier, Emission characterization of a single CdSe-ZnS nanocrystal with high temporal and spectral resolution by photon-correlation fourier spectroscopy, *Phys. Rev. Lett.*, 2008, 100(2): 027403
55. V. D. Kulakowski, B. Bacher, R. Weigand, T. Kümmel, A. Forchel, E. Borovitskaya, K. Leonardi, and D. Hommel, Fine structure of biexciton emission in symmetric and asymmetric cdse/znse single quantum dots, *Phys. Rev. Lett.*, 1999, 82(8): 1780
56. R. D. Schaller, S. A. Crooker, D. A. Bussian, J. M. Pietryga, J. Joo, and V. I. Klimov, Revealing the exciton fine structure of PbSe nanocrystal quantum dots using optical spectroscopy in high magnetic fields, *Phys. Rev. Lett.*, 2010, 105(6): 067403
57. M. Yamaguchi, T. Asano, K. Kojima, and S. Noda, Quantum electrodynamics of a nanocavity coupled with exciton complexes in a quantum dot, *Phys. Rev. B*, 2009, 80(15): 155326
58. S. M. Ulrich, M. Benyoucef, P. Michler, N. Baer, P. Gartner, F. Jahnke, M. Schwab, H. Kurtze, M. Bayer, S. Farad, Z. Wasilewski, and A. Forchel, Correlated photon-pair emission from a charged single quantum dot, *Phys. Rev. B*, 2005, 71(23): 235328
59. A. Mueller, E. B. Flagg, P. Bianucci, X. Wang, D. G. Deppe, W. Ma, J. Zhang, G. J. Salamo, M. Xiao, and C. K. Shih, Resonance fluorescence from a coherently driven semiconductor quantum dot in a cavity, *Phys. Rev. Lett.*, 2007, 99(18): 187402
60. A. Kuhn, M. Hennrich, and G. Rempe, Deterministic single-photon source for distributed quantum networking, *Phys. Rev. Lett.*, 2002, 89(6): 067901
61. N. Le Thomas, U. Woggon, O. Schops, M. V. Artemyev, M. Kazes, and U. Banin, Cavity QED with semiconductor nanocrystals, *Nano Lett.*, 2006, 6(3): 557
62. K. Hennessy, A. Badolato, M. Winger, D. Gerace, M. Atature, S. Gulde, S. Falt, E. L. Hu, and A. Imamolu, Quantum nature of a strongly coupled single quantum dot–cavity system, *Nature*, 2007, 445(7130): 896
63. Y. Ota, M. Nomura, N. Kumagai, K. Watanabe, S. Ishida, S. Iwamoto, and Y. Arakawa, Enhanced photon emission and absorption of single quantum dot in resonance with two modes in photonic crystal nanocavity, *Appl. Phys. Lett.*, 2008, 93(18): 183114
64. E. Pelucchi, S. Watanabe, K. Leifer, Q. Zhu, B. Dwir, P. De Los Rios, and E. Kapon, Mechanisms of quantum dot energy engineering by metalorganic vapor phase epitaxy on patterned nonplanar substrates, *Nano Lett.*, 2007, 7(5): 1282
65. C. Schneider, T. Heindel, A. Huggenberger, P. Weinmann, C. Kistner, M. Kamp, S. Reitzenstein, S. Hofling, and A. Forchel, Single photon emission from a site-controlled quantum dot-micropillar cavity system, *Appl. Phys. Lett.*, 2009, 94(11): 111111
66. P. Gallo, M. Felici, B. Dwir, K. A. Atlasov, K. F. Karlsson, A. Rudra, A. Mohan, G. Biasiol, L. Sorba, and E. Kapon, Integration of site-controlled pyramidal quantum dots and photonic crystal membrane cavities, *Appl. Phys. Lett.*, 2008, 92(26): 263101
67. M. Poitras, C. B. Lipson, H. Du, M. A. Hahn, and T. D. Krauss, Photoluminescence enhancement of colloidal quantum dots embedded in a monolithic microcavity, *Appl. Phys. Lett.*, 2003, 82(23): 4032
68. L. Martidadonna, L. Carbone, M. De Giorgi, L. Manna, G. Gigli, R. Cingolani, and M. De Vittorio, High Q-factor colloidal nanocrystal-based vertical microcavity by hot embossing technology, *Appl. Phys. Lett.*, 2006, 88(18): 181108

69. M. V. Artemyev, U. Woggon, R. Wannemacher, H. Jaschinski, and W. Langbein, Light trapped in a photonic dot: Microspheres act as a cavity for quantum dot emission, *Nano Lett.*, 2001, 1(6): 309

70. A. Qualtieri, G. Morello, P. Spinicelli, M. T. Todaro, T. Stomeo, L. Martiradonna, M. De Giornia, X. Quelinc, S. Builc, A. Bramati, J. P. Hermier, R. Cingolani, and M. De Vittorio, Room temperature single-photon sources based on single colloidal nanocrystals in microcavities, *Superlattices Microstruct.*, 2010, 47(1): 187

71. F. Pisanello, A. Qualtieri, G. Leménager, L. Martiradonna, T. Stomeo, R. Cingolani, A. Bramati, and M. De Vittorio, Single colloidal quantum dots as sources of single photons for quantum cryptography, *Proc. SPIE*, 2011, 7947(1): 794709

72. A. Qualtieri, L. Martiradonna, T. Stomeo, M. T. Todaro, R. Cingolani, and M. De Vittorio, Multicolored devices fabricated by direct lithography of colloidal nanocrystals, *Microelectron. Eng.*, 2009, 86(4): 1127

73. A. Shabaev and A. L. Efros, 1D exciton spectroscopy of semiconductor nanorods, *Nano Lett.*, 2004, 4(10): 1821

74. C. Santori, M. Pelton, G. Solomon, Y. Dale, and Y. Yamamoto, Triggered single photons from a quantum dot, *Phys. Rev. Lett.*, 2001, 86(8): 1502

75. A. Malko, D. Y. Oberli, M. H. Baier, E. Pelucchi, F. Michelini, K. F. Karlson, M. A. Dupertuis, and E. Kapon, Single-photon emission from pyramidal quantum dots: The impact of hole thermalization on photon emission statistics, *Phys. Rev. B*, 2005, 72(19): 195332

76. A. Malko, M. H. Baier, K. F. Karlson, E. Pelucchi, D. Y. Oberli, and E. Kapon, Optimization of the efficiency of single-photon sources based on quantum dots under optical excitation, *Appl. Phys. Lett.*, 2006, 88(8): 081905

77. S. Kiravittaya, M. Benyoucef, R. Zapf-Gottwick, A. Rastelli, and O. G. Schmidt, Ordered GaAs quantum dot arrays on GaAs(001): Single photon emission and fine structure splitting, *Appl. Phys. Lett.*, 2006, 89(23): 233102

78. S. Kimura, H. Kumano, M. Endo, I. Suemune, T. Yokoi, H. Sasakura, S. Adachi, S. Muto, H. Z. Song, S. Hirose, and T. Usuki, Single-photon generation from InAlAs single quantum dot, *Phys. Status Solidi (c)*, 2005, 2(11): 3833

79. M. Bommer, W. M. Schulz, R. Roßbach, M. Jetter, P. Michler, T. Thomay, A. Leitenstorfer, and R. Bratschitsch, Triggered single-photon emission in the red spectral range from optically excited InP/(Al,Ga)InP quantum dots embedded in micropillars up to 100 K, *J. Appl. Phys.*, 2011, 110(6): 063108

80. A. Ugur, S. Kremling, F. Hatami, S. Höfling, L. Worschech, A. Forchel, and W. T. Masselink, Single-photon emitters based on epitaxial isolated InP/InGaP quantum dots, *Appl. Phys. Lett.*, 2012, 100(2): 023116

81. M. B. Ward, O. Z. Karimov, D. C. Unitt, Z. L. Yuan, P. See, D. G. Gevaux, A. J. Shields, P. Atkinson, and D. A. Ritchie, On-demand single-photon source for 1.3 μm telecom fiber, *Appl. Phys. Lett.*, 2005, 86(20): 201111

82. T. Yamaguchi, T. Tawara, H. Kamada, H. Gotoh, H. Okamoto, H. Nakano, and O. Mikami, Single-photon emission from single quantum dots in a hybrid pillar microcavity, *Appl. Phys. Lett.*, 2008, 92(8): 081906

83. S. Strauf, N. G. Stoltz, M. T. Rakher, L. A. Coldren, P. M. Petroff, and D. Boumeester, High-frequency single-photon source with polarization control, *Nat. Photonics*, 2007, 1(12): 704

84. J. Kim, O. Benson, H. Kan, and Y. Yamamoto, A single-photon turnstile device, *Nature*, 1999, 397(6719): 500

85. A. J. Shields, Semiconductor quantum light sources, *Nat. Photonics*, 2007, 1(4): 215

86. A. J. Bennett, D. C. Unitt, P. See, A. J. Shields, P. Atkinson, K. Cooper, and D. A. Ritchie, Electrical control of the uncertainty in the time of single photon emission events, *Phys. Rev. B*, 2005, 72(3): 033316

87. M. B. Ward, T. Farrow, P. See, Z. L. Yuan, O. Z. Karimov, P. Atkinson, K. Cooper, and D. A. Ritchie, Electrically driven telecommunication wavelength single-photon source, *Appl. Phys. Lett.*, 2007, 90(6): 063512

88. T. Heindel, C. Schneider, M. Lermer, S. H. Kwon, T. Braun, S. Reitzenstein, S. Höfling, M. Kamp, and A. Forchel, Electrically driven quantum dot-micropillar single photon source with 34% overall efficiency, *Appl. Phys. Lett.*, 2010, 96(1): 011107

89. D. J. Ellis, A. J. Bennett, A. J. Shields, P. Atkinson, and D. A. Ritchie, Electrically addressing a single self-assembled quantum dot, *Appl. Phys. Lett.*, 2006, 88(13): 133509

90. M. Scholz, S. Büttner, O. Benson, A. I. Toropov, A. K. Bakarov, A. K. Kalagin, A. Lochmann, E. Stock, O. Schulz, F. Hopfer, V. A. Haisler, and D. Bimberg, Non-classical light emission from a single electrically driven quantum dot, *Opt. Express*, 2007, 15(15): 9107

91. D. J. P. Ellis, A. J. Bennett, S. J. Dewhurst, C. A. Nicoll, D. A. Ritchie, and A. J. Shields, Cavity-enhanced radiative emission rate in a single-photon-emitting diode operating at 0.5 GHz, *New J. Phys.*, 2008, 10(4): 043035

92. M. Reischle, G. J. Beirne, W. M. Schulz, M. Eichfelder, R. Rosbach, M. Jetter, and P. Michler, Electrically pumped single-photon emission in the visible spectral range up to 80 K, *Opt. Express*, 2008, 16(17): 12771

93. P. Ester, L. Lackmann, S. Michaelis de Vasconcellos, M. C. Hübner, A. Zrenner, and M. Bichler, Single photon emission based on coherent state preparation, *Appl. Phys. Lett.*, 2007, 91(11): 111110

94. D. Press, S. Gtzinger, S. Reitzenstein, C. Hofmann, A. Lffler, M. Kamp, A. Forchel, and Y. Yamamoto, Photon antibunching from a single quantum-dot-microcavity system in the strong coupling regime, *Phys. Rev. Lett.*, 2007, 98(11): 117402

95. S. Kako, C. Santori, K. Hoshino, S. Gtzinger, Y. Yamamoto, and Y. Arakawa, A gallium nitride single-photon source operating at 200 K, *Nat. Mater.*, 2006, 5(11): 887

96. R. Arians, T. Kmmell, G. Bacher, A. Gust, C. Kruse, and D. Hommel, Room temperature emission from CdSe/ZnSSe/MgS single quantum dots, *Appl. Phys. Lett.*, 2007, 90(10): 101114
97. A. Tribu, G. Sallen, T. Aichele, R. André, J. P. Poizat, C. Bougerol, S. Tatarenko, and K. Kheng, A high-temperature single-photon source from nanowire quantum dots, *Nano Lett.*, 2008, 8(12): 4326
98. A. F. Jarjour, R. A. Oliver, R. A. Taylor, Nitride-based quantum dots for single photon source applications, *physica status solidi (a)*, 2009, 206(11): 2510
99. O. Fedorych, C. Kruse, A. Ruban, D. Hommel, G. Bacher, and T. Kümmell, Room temperature single photon emission from an epitaxially grown quantum dot, *Appl. Phys. Lett.*, 2012, 100(6): 061114
100. B. S. Song, S. Noda, T. Asano, and Y. Akahane, Ultra-high-*Q* photonic double-heterostructure nanocavity, *Nat. Mater.*, 2005,4(3): 207
101. W. L. Yang, Z. Q. Yin, Z. Y. Xu, M. Feng, and C. H. Oh, Quantum dynamics and quantum state transfer between separated nitrogen-vacancy centers embedded in photonic crystal cavities, *Phys. Rev. A*, 2011, 84(4): 043849
102. S. John, Strong localization of photons in certain disordered dielectric superlattices, *Phys. Rev. Lett.*, 1987, 58(23): 2486
103. L. Florescu, Nonclassical light generation by a photonic-crystal one-atom laser, *Phys. Rev. A*, 2008, 78(2): 023827
104. M. I. Makin, J. H. Cole, C. Tahan, L. C. L. Hollenberg, and A. D. Greentree, Quantum phase transitions in photonic cavities with two-level systems, *Phys. Rev. A*, 2008, 77(5): 053819
105. S. Hughes, L. Ramunno, J. F. Young, and J. E. Sipe, Extrinsic optical scattering loss in photonic crystal waveguides: Role of fabrication disorder and photon group velocity, *Phys. Rev. Lett.*, 2005, 94(3): 033903
106. M. G. Banaee, A. G. Pattantyus-Abraham, M. W. Mccutcheon, G. W. Rieger, and J. F. Young, Efficient coupling of photonic crystal microcavity modes to a ridge waveguide, *Appl. Phys. Lett.*, 2007, 90(19): 193106
107. P. Yao, and S. Hughes, Controlled cavity-QED using a planar photonic crystal waveguide-cavity system, arXiv: 0904.4469v2, 2009
108. V. S. C. Manga Rao, and S. Hughes, Numerical study of exact Purcell factors in finite-size planar photonic crystal waveguides, *Opt. Lett.*, 2008, 33(14): 1587
109. R. Bose, K. Roy, T. Cai, G. S. Solomon, and E. Waks, APS March Meeting 2013, 58(1): A26.00009
110. A. Faraon, A. Majumdar, H. Kim, P. Petroff, and J. Vuckovic, Fast electrical control of a quantum dot strongly coupled to a photonic-crystal cavity, *Phys. Rev. Lett.*, 2010, 104(4): 047402
111. E. D. Kim, K. Truex, X. Xu, B. Sun, D. G. Steel, A. S. Bracker, D. Gammon, and L. J. Sham, Fast spin rotations by optically controlled geometric phases in a charge-tunable inas quantum dot, *Phys. Rev. Lett.*, 2010, 104(16): 167401
112. B. Ellis, M. A. Mayer, G. Shambat, T. Sarmiento, J. Harris, E. E. Haller, and J. Vučković, Ultralow-threshold electrically pumped quantum-dot photonic-crystal nanocavity laser, *Nat. Photonics*, 2011, 5: 297